Impact dynamic response of low damped structures subjected to impulse base accelerations

Andrés García-Pérez[a,*], Giuliano Coppotelli[b], Gustavo Alonso[a]

[a] Instituto Universitario de Microgravedad "Ignacio Da Riva" (IDR), Escuela Técnica Superior de Ingeniería Aeronáutica y del Espacio (ETSIAE), Universidad Politécnica de Madrid (UPM), Pza. Cardenal Cisneros 3, 28040 Madrid, Spain

[b] Department of Mechanical and Aerospace Engineering, Università di Roma "La Sapienza", Via Eudossiana 18, 00184 Rome, Italy

[*]Corresponding author: andres.garcia.perez@upm.es

Abstract

Shocks and impact loads are generated during the operational life of aerospace vehicles and their effects should be considered for the structural design and verification of these systems. Due to the complexity of assessing shock loads numerically, there is a lack of accurate methods to calculate the mechanical response under a shock environment. One of the existing approaches is the Response Spectrum Analysis, which directly estimates the maximum peak values of structural response accelerations generated by shocks, where it is necessary to define the input acceleration as a Shock Response Spectrum. This approach is based on the calculation of the modal contributions to the total maximum response, which can be combined in different ways, leading to a great variety of possible results for the same response. Furthermore, the existing options generally provide inaccurate results. The objective of this paper is the development and verification of a new method for the Response Spectrum Analysis approach to calculate accurately the peak response accelerations of undamped and low damped structures subjected to impulse base excitations characterized by a main pulse. The proposed method is verified in this paper by numerical analyses for a beam structure to demonstrate the improvement in the accuracy of the provided results compared to the existing options.

Keywords: finite element, response spectrum analysis, shock, shock response spectrum, structural analysis

1 Introduction

Airplanes, spacecraft and rockets are subjected to a wide variety of mechanical loads generated by both their internal operations and external conditions. For the structural design and verification of these systems, these varied mechanical loads are classified into different categories according to their characteristics in terms of time variability (static versus dynamic), frequency content and transient or permanent character, to be later evaluated separately in representative tests and numerical simulations [1,2]. One of the most important load cases is the shock, which is defined as a transient load with high intensity and short duration [2,3]. Due to these characteristics, especially the transient behavior, the mechanical assessment of structures subjected to shock loads has been difficult to carry out because of the complexity in the definition and in the mathematical treatment of this type of loads. However, the demand of numerical analyses to assess the effects of shocks on aerospace structures is currently increasing, as in the example of the Energetic Particle Detector (EPD) payload units for the Solar Orbiter space mission [4], where the capability of these units to withstand the specified shock loads was demonstrated by numerical analysis. An overview of existing numerical methods for shock simulations is reported in [5], where the accuracy of the calculated results is evaluated with the numerical model of Supra Thermal Electrons and Protons (STEP) instrument for the Solar Orbiter spacecraft. This study revealed the great variety of different options for the numerical shock simulations, including the transient analysis and the Response Spectrum Analysis (RSA), and the low accuracy in the results of most of them. Recent studies have improved the level of accuracy of numerical analysis for the shock assessment, most of them based on transient analysis. In [6], new techniques to represent the input acceleration field measured in impact tests of space instruments with a higher level of accuracy in transient analysis were developed and validated achieving a great correlation with the experimental results. In [7], an improved numerical technique that combines two different approaches (finite element and statistical energy analysis) is used to enhance the accuracy of the shock response of spacecraft structures calculated by numerical simulations. In [8], the employed numerical simulations were demonstrated to have the sufficient accuracy to simulate the shock effects on the separation systems that allow the release of spacecraft at the end of the launch phase, where the influence of their design parameters on the mitigation of the transmitted shock were evaluated. One of the key parameters of the shock simulations is the damping of the analyzed structure, which has been evaluated in different works [9-11] with the aim of having a more accurate damping definition in transient analyses to obtain reliable and accurate results.

The approach used in this paper for the numerical analysis of shock loads is the Response Spectrum Analysis, which is a method that consists of the direct determination of the maximum peaks of acceleration response of a system subjected to a dynamic base excitation. It is an alternative method to the transient analysis with the main advantage of obtaining results in less computational time. This method was initially developed for the calculation of the effects of earthquakes on buildings [12], but it was later adapted in the aerospace industry to represent the effects of shock loads on airplanes, rockets and spacecraft structures. What differentiates shock loads from other dynamic loads is their transient nature, high level of amplitude and short duration. These characteristics imply that the mathematical treatment of shock loads is more complex than for other mechanical loads, which generates a higher level of uncertainty in the structural results. The adopted criterion in the European space industry to define the input shock levels is the Shock Response Spectrum (SRS), which is the graphical

representation of the absolute maximum level of response acceleration (peak value) of a single degree of freedom (SDOF) system subjected to a shock base excitation as a function of its natural frequency and for a given damping ratio (typically $\zeta = 0.05$) of the SDOF system [3]. To improve the representation of the effects of the shock load with the SRS, it is recommended to consider more than one damping ratio, where each one is represented by a curve in the SRS, as can be seen in the example in Figure 1. In this figure, the amplification factor $Q = 1 / 2\zeta$ is used instead of the damping ratio to identify each curve, where the levels of the curves are higher for higher values of amplification factor.

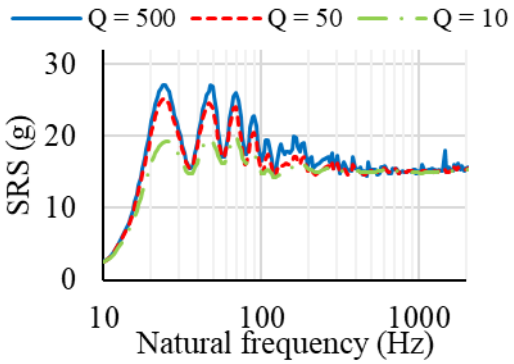

Figure 1: Example of an SRS representation with three curves associated with different amplification factors.

If the analyzed model subjected to a shock base excitation corresponds to a SDOF system with known viscous damping, the peak value of acceleration response is directly determined from the SRS by looking for the point just at its natural frequency of the curve associated with the given damping or amplification factor. However, real structures are much more complex than a simple SDOF system, involving more than one natural frequency within the frequency range of interest and possibly with different damping values associated to the different natural frequencies. This fact implies that the calculation of the response of multiple degree of freedom (MDOF) systems is more difficult and with a greater uncertainty than for SDOF systems.

To analyze a MDOF system in a RSA simulation, it is preferable to use the finite element analysis (FEA) approach, which is the most widely used technique for the numerical simulations of the mechanical effects caused by dynamic loads on space structures, with NASTRAN being the preferred software tool for the structural analysis in the European projects [13].

The principle of modal superposition of linear systems for modal transient analyses implies that the physical response acceleration at any given point of the structure ($\ddot{x}_j$) is the sum of the modal responses ($\ddot{y}_{ij}$) of all the involved modes (M modes), as it is indicated in the next equation, where $\ddot{\eta}_i$ is the response acceleration of each modal coordinate considered as a SDOF system, Γ_i is the modal participation factor of the mode i and ϕ_{ij} is the component j of the eigenvector of the mode i.

$$\ddot{x}_j(t) = \sum_{i=1}^{M} \ddot{y}_{ij}(t) = \sum_{i=1}^{M} \phi_{ij} \Gamma_i \ddot{\eta}_i(t) \qquad (1)$$

When the model is analyzed in an RSA simulation, the peak of each modal response (${\ddot{y}_{ij}}^{peak}$) is calculated according to the next equation, where the factor $SRS\,(f_i)$ corresponds to the value of the input SRS at the natural frequency f_i and defined at the corresponding damping value associated to this mode. If the input SRS curves are related to other damping values, the used $SRS\,(f_i)$ value is determined by interpolating from these input SRS curves.

$$ {\ddot{y}_{ij}}^{peak} = \phi_{ij}\Gamma_i{\ddot{\eta}_i}^{peak} = \phi_{ij}\Gamma_i SRS(f_i) \tag{2} $$

The next step in the RSA simulation is to add all the modal contributions to calculate directly the peak value of the physical acceleration (${\ddot{x}_j}^{peak}$) of the degree of freedom j, which can be done with the different options described below [1], where each one is related to different assumptions with the aim of simplifying the calculation to combine the modal contributions:

- ABS: This option considers that the maximum peak values from the modal response accelerations occur at the same instant and with the same sign, so it represents the worst case in terms of total maximum response.
- SRSS: This option assumes that the peaks of the modal response accelerations occur at different instants of time, so that the peak value of the total physical response can be estimated as the Square Root of the Summation of Square (SRSS) peak values of each modal response.
- NRL: This option, developed by the Naval Research Laboratory (NRL), is a compromise between the two previous options, where the total peak response is the sum of the absolute value of the highest modal response and the SRSS calculation of the rest of modal responses. The assumption behind this option is that the maximum response in many cases is due mainly to the highest modal contribution of a single mode, while the rest of modal responses contribute less, which are included as a SRSS summation.
- CQC: This option is the Complete Quadratic Combination (CQC) and consists of a variant of the SRSS option, where the cross influence between the different modes is considered by the parameter of the cross-modal (covariance) coefficient p_{ik}. This option considers that the mutual influence between each pair of modes is also important to the total response, leading to higher maximum peak values than the SRSS option.

The equations related to the different options are shown in Table 1. It is assumed in these equations that there are M modes within the frequency range of interest, covered by the input SRS curves.

Table 1: Equations of the different summation options for the RSA method.

Option	Equation
ABS	$\ddot{x}_j^{peak} = \sum_{i=1}^{M} \left\lvert \phi_{ij} \Gamma_i SRS(f_i) \right\rvert$
SRSS	$\ddot{x}_j^{peak} = \sqrt{\sum_{i=1}^{M} \left(\phi_{ij} \Gamma_i SRS(f_i) \right)^2}$
NRL	$\ddot{x}_j^{peak} = \left\lvert \phi_{kj} \Gamma_k SRS(f_k) \right\rvert + \sqrt{\sum_{\substack{i=1 \\ i \neq k}}^{M} \left(\phi_{ij} \Gamma_i SRS(f_i) \right)^2}$
CQC	$\ddot{x}_j^{peak} = \sqrt{\sum_{i=1}^{M} \sum_{k=1}^{M} \left(\phi_{ij} \Gamma_i SRS(f_i) \right) p_{ik} \left(\phi_{kj} \Gamma_k SRS(f_k) \right)}$

As it was demonstrated in [5], the RSA method has low accuracy and wide scattering of the results for the same response calculated with the different summation options. These existing options generally provide unreliable and inaccurate results because they are based on weak assumptions that do not take into account the particularities of the different shocks. These existing options try to be applicable to any type of load condition, but actually, they cannot predict the results with sufficient accuracy in any case. The reason is that despite they predict accurately the maximum value for each modal contribution (see Eq. (2)), they cannot predict the instants of time in which each maximum value appears. Consequently, the summations of all the modal contributions are done in very inaccurate ways for the existing options.

New summation options for the RSA simulations have been developed in recent studies, such as the Complex Complete Quadratic Combination (CCQC) option defined in [14], which is a variation of the CQC option but for non-classically damped structures. This option was improved in subsequent works, such as in [15], where a simplified CCQC was proposed to enhance the computational efficiency of the peak acceleration responses, and in [16], where an alternative option was developed to be used in MDOF systems with repeated eigenvalues. In [17], the accuracy of the CCQC option was improved by a modification that takes the high-frequency modes into account in a different way, resulting in more accurate calculations for the peak values of the response accelerations of damped systems. In [18], a new method is proposed to predict the peak values of the response acceleration of structures subjected to impact loads by using a new concept that combines the SRS with the low-pass and band-pass filtering of the acceleration signals.

This paper proposes and verifies a new summation option for undamped and low damped structures with the objective of determining the peak values of the response accelerations in a more accurate way than the existing options. The application of this method is limited to shock impacts with an input acceleration whose profile is characterized by a main pulse that can be defined with different shapes (half-sine, rectangular, triangular…), which is a standardized way for the shock tests employed to

qualify electronic equipment [2]. The option proposed in this study achieves higher accuracy than the existing options for the particular case of low damped structures subjected to an impact load characterized by a main pulse. This is because it has been created with strong assumptions that improve the representability of the involved physical phenomena by the proposed equations, where the different possibilities about the instants of time in which the maximum peaks of modal responses are produced are taken into account by classifying the modal responses according to different categories. The drawback of the proposed method is its narrow valid range of applicability, which is reduced to the case of low damping structures subjected to shocks defined by a main input pulse, but which can be useful in many applications considering that this type of load is widely used in the aerospace industry. The proposed method and its hypotheses are explained in Section 2, together with the descriptions of the test setup and the numerical model. The results used to verify the proposed method are detailed in Section 3, and the conclusions are exposed in Section 4.

2 Methodology

2.1 Proposed method for the Response Spectrum Analysis

The proposed method is named of "Impact Dynamic Response of Undamped Physical Models" (IDR-UPM) and has been developed by considering the next assumptions, which are demonstrated in this paper by experimental and numerical results of a representative structure subjected to different shock tests. The hypotheses applied to the IDR-UPM option are the following:

- The analyzed structure presents very low damping values associated with the involved modes, so it can be considered as an undamped structure to simplify the calculation.
- This method has been verified in this work for input shocks characterized by a main pulse, which is accompanied by a pre-pulse and a post-pulse that are needed to achieve zero end for the displacement and velocity functions during the tests.
- The modal responses generated by an impact defined by a main pulse are classified into three categories depending on the value of the corresponding natural frequency with respect to the frequency content associated to the input shock. The first category corresponds to modes with very low natural frequencies, far below the frequency content of the input shock, whose modal responses can be considered negligible. The second category corresponds to modes with natural frequencies within the frequency range of the input load, where each modal response is characterized by a sinusoidal function at the corresponding natural frequency, where the maximum and minimum peaks are periodically repeated with very low decay (zero decay for undamped structures). The third category corresponds to modes with natural frequencies above the frequency content of the input shock, where the modal responses have the same shape as the input acceleration (the maximum peaks of the responses occur at practically the same instant as the maximum value of the main pulse) but with different scale factors and signs.
- Taking into account the assumptions of the previous point, there are two possible options to find the peak value of the total response acceleration at a given point of the analyzed structure. The first possibility is that the peak value occurs during the main input pulse, dominated by the modal responses of the

modes belonging to the third category. The second possibility is that the peak value occurs at any instant after the main pulse, dominated by the modal responses of the modes of the second category. In this case, it is difficult to exactly know the instant when this peak appears, but taking into account the periodicity of the sinusoidal time functions of the modal responses, there will probably be a moment in which the maximum peaks of the main modal responses coincide at the same instant and with the same sign, which allows the estimation of the total peak value as the summation of the absolute maximum values of the modal contributions of the involved modes.

Considering the mentioned hypotheses, the IDR-UPM method is defined by the following set of equations.

$$\ddot{x}_j^{peak} = \max\left(\ddot{x}_j^{pulse}, \ddot{x}_j^{post}\right) \tag{3}$$

$$\ddot{x}_j^{post} = \sum_{m_1}^{m_2} \left|\phi_{ij}\Gamma_i SRS(f_i)\right| + K_1 \sum_{m_2}^{m_3} \left|\phi_{ij}\Gamma_i SRS(f_i)\right| \tag{4}$$

$$\ddot{x}_j^{pulse} = \left|\sum_{m_1}^{m_2} K_i\phi_{ij}\Gamma_i SRS(f_i) + \sum_{m_2}^{m_e} \phi_{ij}\Gamma_i SRS(f_i)\right| \tag{5}$$

The indexes m_1, m_2 and m_3 are related to the frequencies of the modes f_1, f_2 and f_3 respectively that define the limits of the different frequency ranges that are explained below. The index m_e is the index for the last mode (f_e) within the frequency range of interest covered by the input SRS curves.

Eq. (3) indicates that the peak value of response acceleration at any point j of the structure is the maximum value between the two considered options: or the peak value occurs during the main pulse or at a later time.

Eq. (4) calculates the maximum peak response that is generated during the time after the application of the main pulse. In this equation, the modal contributions of the modes of the second category, within the frequency range between f_1 and f_2, are added as for the ABS option, while the summation of the modes of the transition region defined within f_2 and f_3 belonging to the third category is carried out in the same way, but with the application of a correction factor K_1 that multiplies this second summation. This correction factor is related to a particular characteristic of the modal responses of the modes of this transition region and its value is estimated as the average ratio between the oscillation amplitude of the responses after the input pulse and the maximum peaks of the responses generated during the input pulse. The contribution of the modes outside the frequency range between f_1 and f_3 is considered negligible. The determination of these limits (f_1, f_2 and f_3) for the frequency ranges and of the correction factor are explained later in this paper.

Eq. (5) estimates the maximum peak value of the response when it occurs at the same instant as the maximum value of the input main pulse. The peak response is considered as the absolute value of the sum of the modal responses of the modes belonging to the

second category (between f_1 and f_2) and to the third category (between f_2 and the maximum frequency of interest f_e). In this case, the modal contributions are summed algebraically. Additionally, there are correction factors K_i applied only to the modal responses of the modes of the second category, because their peak values may not occur at the same instant as the maximum value of the input pulse. Therefore, the values of these correction factors must be the relationship between the value of the corresponding modal response at the considered instant and its absolute maximum value, which appears at a different time.

2.2 Tests description and results

The analyzed structure is a cantilevered thin-walled beam made of aluminum alloy (E = 70 GPa, ν = 0.33, ρ = 2700 kg/m^3), which is clamped at its lower end by a set of mechanical pieces that hold and connect it to the slip table of the shaker. The vertical beam (Figure 2) is made up of a lower section of 40 x 50 mm and 7 mm of thickness, which is the zone in contact with the mechanical fixtures, and an upper section of 220 x 50 mm and 1.5 mm of thickness, which is the free-motion zone. The mechanical assembly that includes the tested beam and the mechanical fixtures is shown in Figure 3, while the test equipment and setup are shown in Figure 4. The shock tests were conducted at the experimental facilities of the Structural Dynamic Laboratory of the Department of Mechanical and Aerospace Engineering of the University of Rome La Sapienza. The input excitations were executed by an electrodynamic shaker "Dongling Air-Cooled Vibration Test" model ES-6-200 (see Figure 4 (a)), where the input signals and the mechanical responses were defined and recorded by a test controller LMS SCADAS III Duel-Channel. For the tests, input and output accelerations were measured by ceramic shear accelerometers whose characteristics are shown in Table 2. There is one control accelerometer (A1) located on one side of the mechanical fixture to measure the input acceleration, and four accelerometers (A2 – A5) located on the tested beam to measure its mechanical response (see Figure 4(b)). Two of these accelerometers (A2 and A3) are symmetrically placed at the top end of the beam, while the other two sensors (A4 and A5) are symmetrically located at the middle of the beam. The results that are compared between experimental and numerical data correspond to the accelerations measured in these points.

Table 2: Accelerometers characteristics.

Mass:	0.5 gm
Sensitivity:	10 mV/g
Measure range:	±500 g pk
Broadband resolution:	0.005 g rms
Frequency range:	1 – 10000 Hz

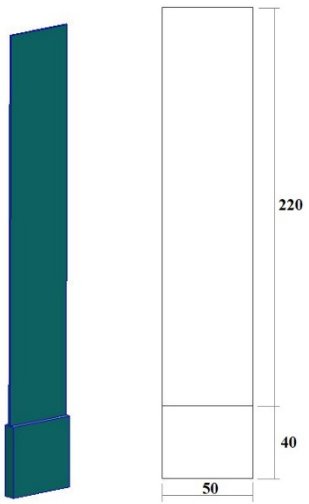

Figure 2: Tested vertical thin beam design and dimensions in millimeters.

Figure 3: Mechanical assembly with the tested vertical beam and the mechanical fixtures.

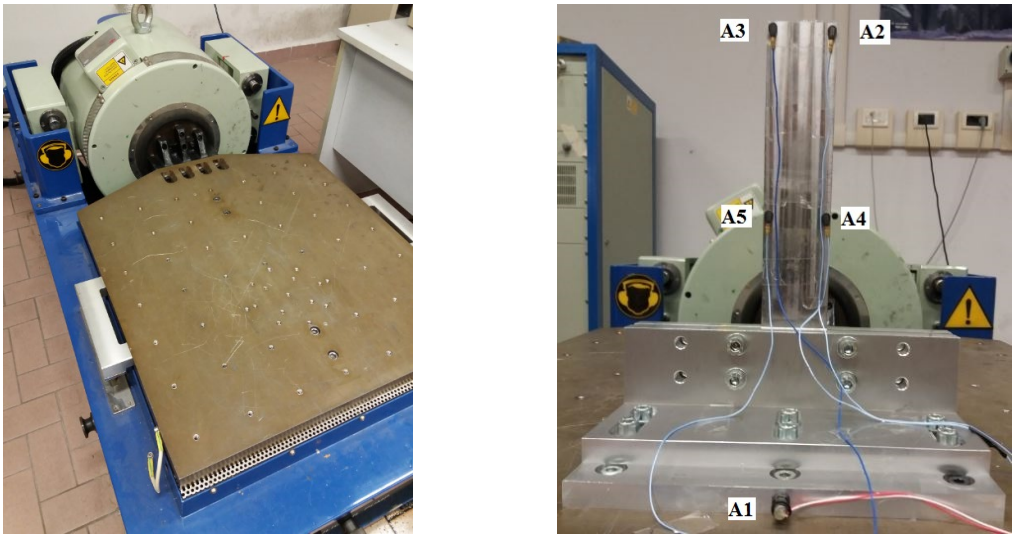

(a) Electrodynamic shaker with slip table (b) Tested assembly with accelerometers

Figure 4: Test equipment and setup for the shock tests of the vertical beam.

In this study, different shock tests were executed by the shaker, each one defined by an input acceleration signal composed of a main pulse accompanied by a pre pulse and a post pulse, as can be seen in Figure 5 as an example. These secondary pulses are necessary to achieve that the acceleration, velocity and displacement signals go to zero at the end of each shock test.

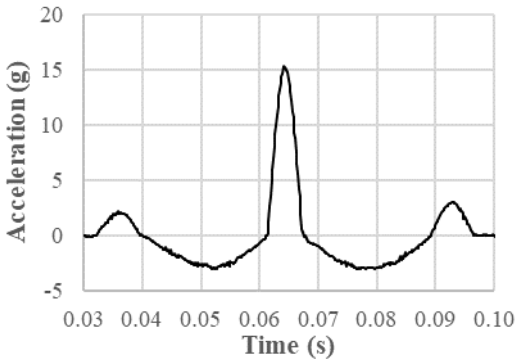

Figure 5: Example of an input acceleration signal defined by a main half-sine pulse of 15 g of amplitude and 6 ms of duration accompanied by a pre-pulse and a post-pulse.

The different input signals correspond to all the combinations of the three proposed shapes for the main pulse (half-sine, rectangular and terminal peak sawtooth), with three amplitude levels (15, 10 and 5 g) and with four durations of the main pulse (11, 6, 3 and 1.5 ms), giving a total of 36 load cases. However, the strictest combination (rectangular pulse with the maximum amplitude (15 g) and the maximum duration (11 ms)) was not finally executed because it exceeded the load capacity of the shaker.

From these shock tests, the response accelerations are obtained to evaluate the influence of the input characteristics on the mechanical responses and to measure the structural properties of the tested beam, such as the natural frequencies and the corresponding modal damping. Some of the experimental results can be seen in Figure 6 and Figure 7, where the time acceleration functions of the responses are shown together with the corresponding input signals.

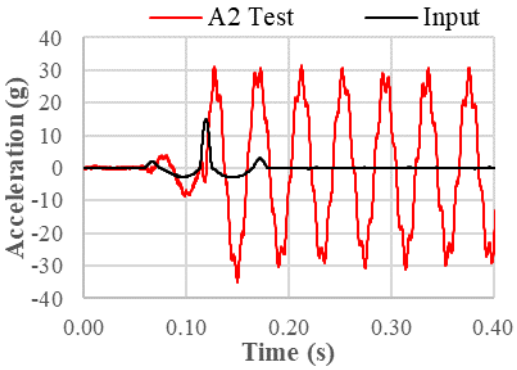

(a) A2 and input signals

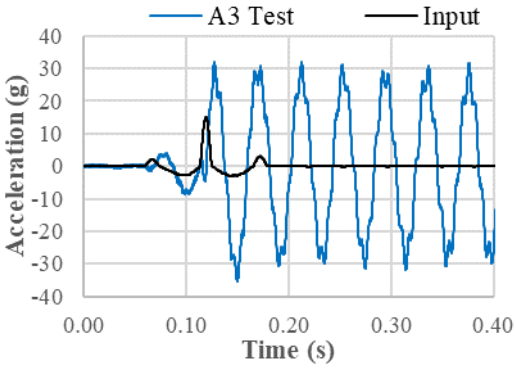

(b) A3 and input signals

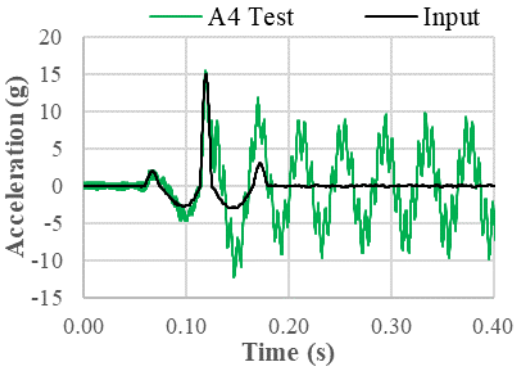

(c) A4 and input signals

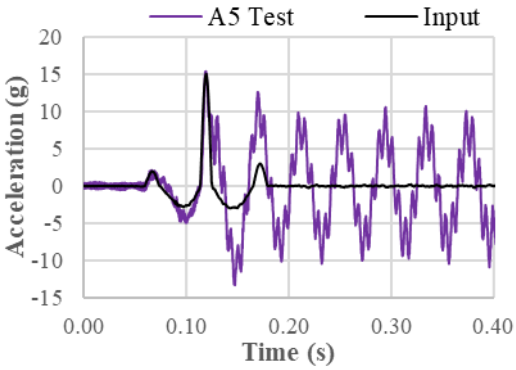

(d) A5 and input signals

Figure 6: Experimental results for the load case of Half-sine pulse of 15 g and 11 ms.

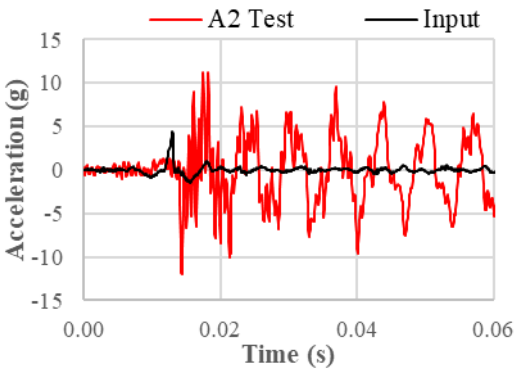

(a) A2 and input signals

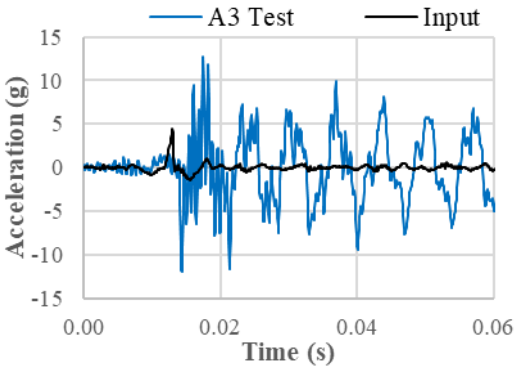

(b) A3 and input signals

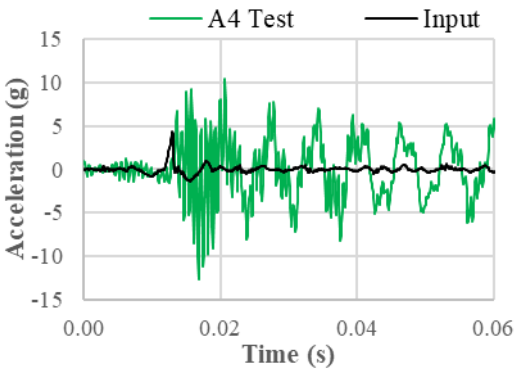

(c) A4 and input signals

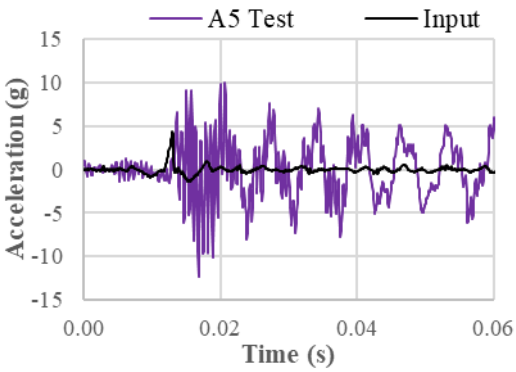

(d) A5 and input signals

Figure 7: Experimental results for the load case Terminal peak sawtooth pulse of 5 g and 1.5 ms.

It can be noticed from these figures the great similarity between the response signals measured by the accelerometers located in symmetrical locations, that is, between A2

and A3 and between A4 and A5. This aspect can be explained by the fact that the mechanical response of the tested beam is dominated by its bending modes, which generate the same results for each set of points located at the same height. Another interesting point is the similarity between the responses when comparing the load cases with the same shape and duration for the input pulse, but with different amplitudes. If the responses are scaled to the same intensity (by dividing by the nominal input level: 15, 10 or 5 g), the similarity can be seen clearly, as shown in Figure 8 for the dimensionless responses measured by the A2 accelerometer in different load cases.

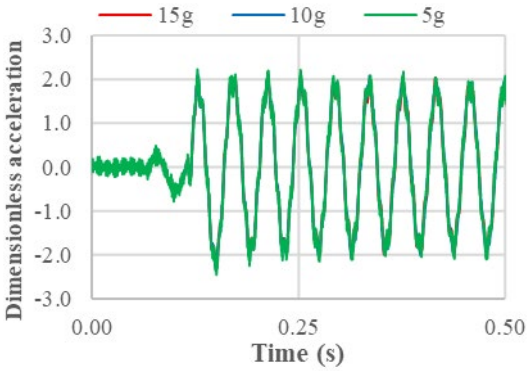

(a) Half-sine 11 ms – A2 scaled signals

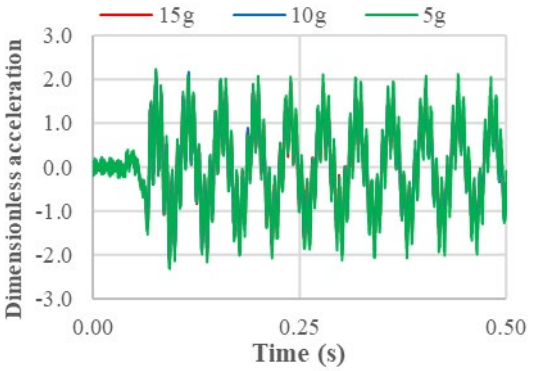

(b) Half-sine 6 ms – A2 scaled signals

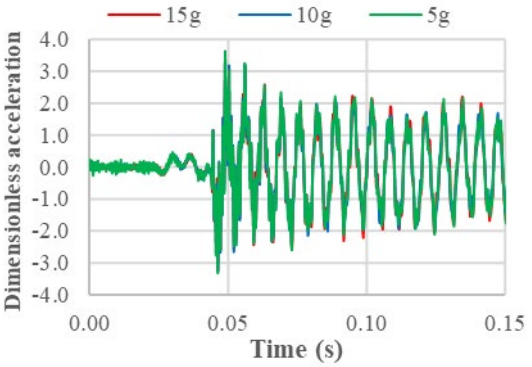

(c) Rectangular 3 ms – A2 scaled signals

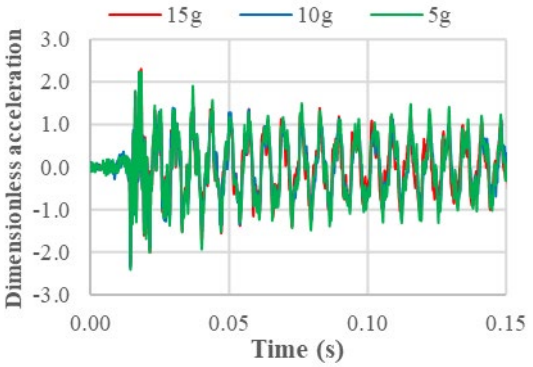

(d) Terminal 1.5 ms – A2 scaled signals

Figure 8: Scaled response signals measured by the A2 accelerometer in different load cases.

With the aim of obtaining the experimental natural frequencies of the tested beam, the time functions are converted by the Fast Fourier Transform (FFT) into spectra defined in the frequency domain. The resulting FFT curves are shown in Figure 9, Figure 10 and Figure 11 for the different load cases, where the input (A1) and the response (A2 and A4) spectra are represented together, but in different scales, to see more clearly the influence of the input frequency content on the excitation of the modes, which are identified in the peaks of the response FFT curves.

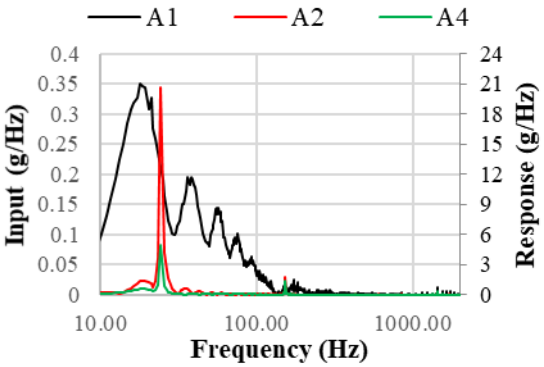

(a) Half-sine 15 g 11 ms

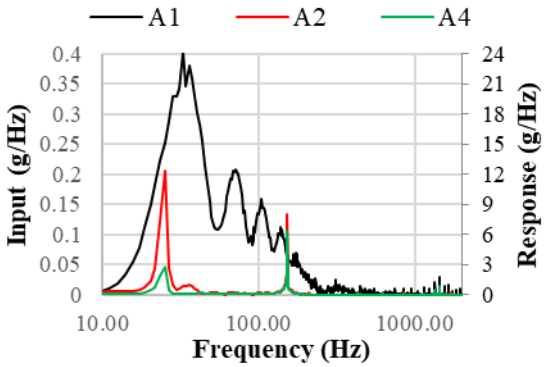

(b) Half-sine 15 g 6 ms

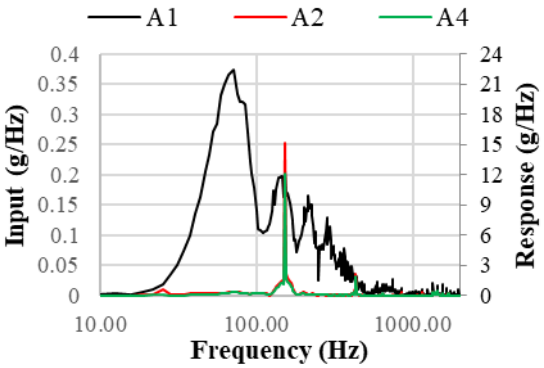

(c) Half-sine 15 g 3 ms

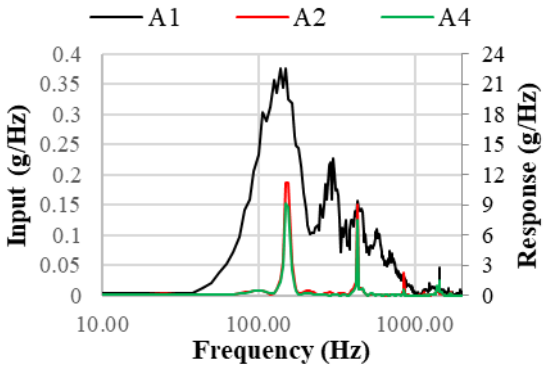

(d) Half-sine 15 g 1.5 ms

Figure 9: FFT curves of the test signals A1 (input), A2 and A4 (responses) for the Half-sine pulse load cases.

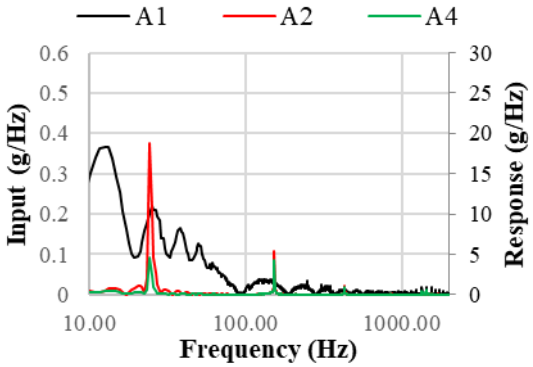

(a) Rectangular 10 g 11 ms

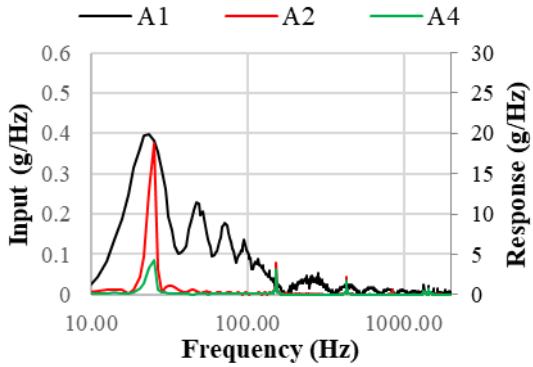

(b) Rectangular 10 g 6 ms

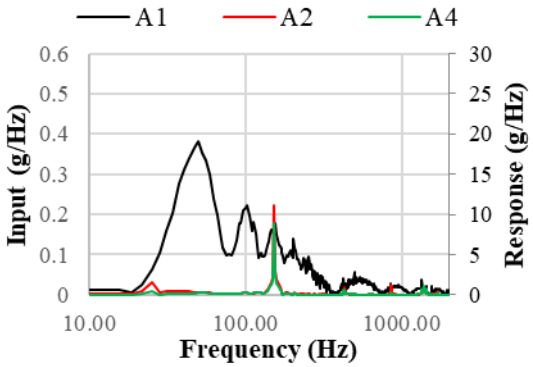

(c) Rectangular 10 g 3 ms

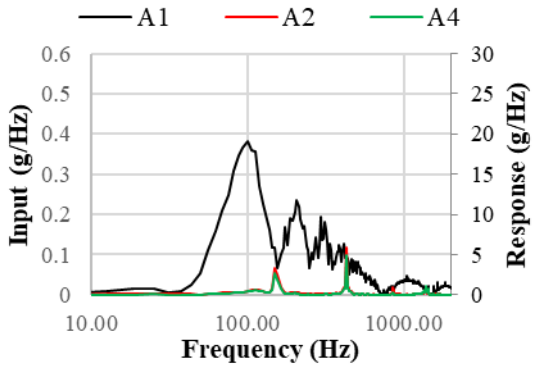

(d) Rectangular 10 g 1.5 ms

Figure 10: FFT curves of the test signals A1 (input), A2 and A4 (responses) for the Rectangular pulse load cases.

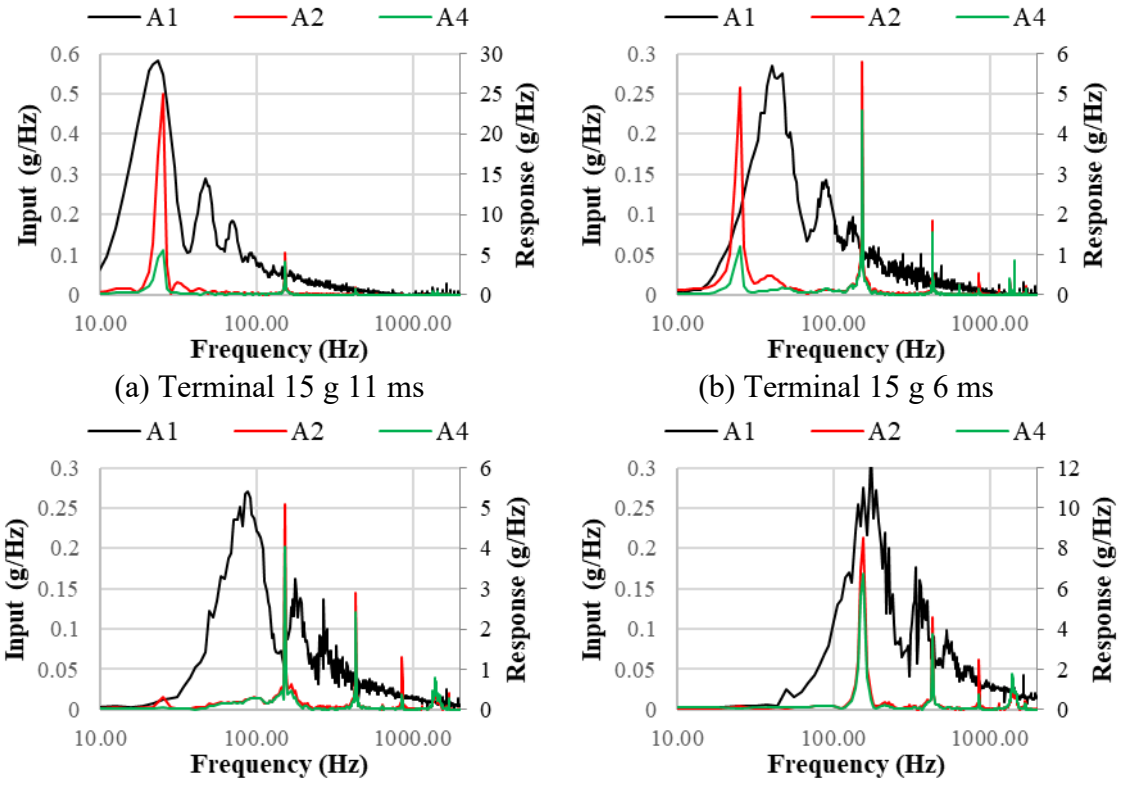

(a) Terminal 15 g 11 ms

(b) Terminal 15 g 6 ms

(c) Terminal 15 g 3 ms

(d) Terminal 15 g 1.5 ms

Figure 11: FFT curves of the test signals A1 (input), A2 and A4 (responses) for the Terminal peak sawtooth pulse load cases.

The shapes of the input FFT functions (A1) are characterized by humps and valleys that decay to zero for high frequencies. These FFT functions clearly indicate the frequency content of the input signals, where for each load case, the input is limited within a frequency band that moves towards higher frequencies for shorter pulses. Consequently, the modes of the tested beam found within each input frequency band are more excited than the modes that are outside, as can be seen in the FFT of the responses in Figure 9, Figure 10 and Figure 11. The FFT curves of the response signals allow the determination of the bending modes of the tested beam, whose frequencies are 24.22, 153.125, 431.25, 856.25 and 1400.0 Hz. The first bending modes are mainly excited by the pulses with longer durations (11 and 6 ms), while the high-frequency modes are excited by the short pulses (3 and 1.5 ms). This fact is also corroborated by observing the period of the sinusoidal time signals in Figure 6 and Figure 7.

The modal viscous damping associated to each mode can be obtained from the experimental results. The employed data processing begins with the band-pass filtering of each response signal at the natural frequency of the most excited mode to obtain a filtered signal that presents a damped sinusoid shape for the time after the application of the input pulse. Due to the wide separation between the natural frequencies of the analyzed structure (see Figure 9, Figure 10 and Figure 11), it was easy to define for each signal a frequency band that only includes the filtered natural frequency, achieving a damped sinusoid at the natural frequency of interest. From this damped sinusoidal signal, the maximum and minimum peaks are extracted to construct the decreasing exponential function that best fits them. Finally, the corresponding damping ratio are calculated from the exponent of this function. In Figure 12, different examples of filtered response signals are shown together with the exponential functions that fit their

maximum and minimum peaks. The resulting experimental natural frequencies and their corresponding damping ratios are shown in Table 3.

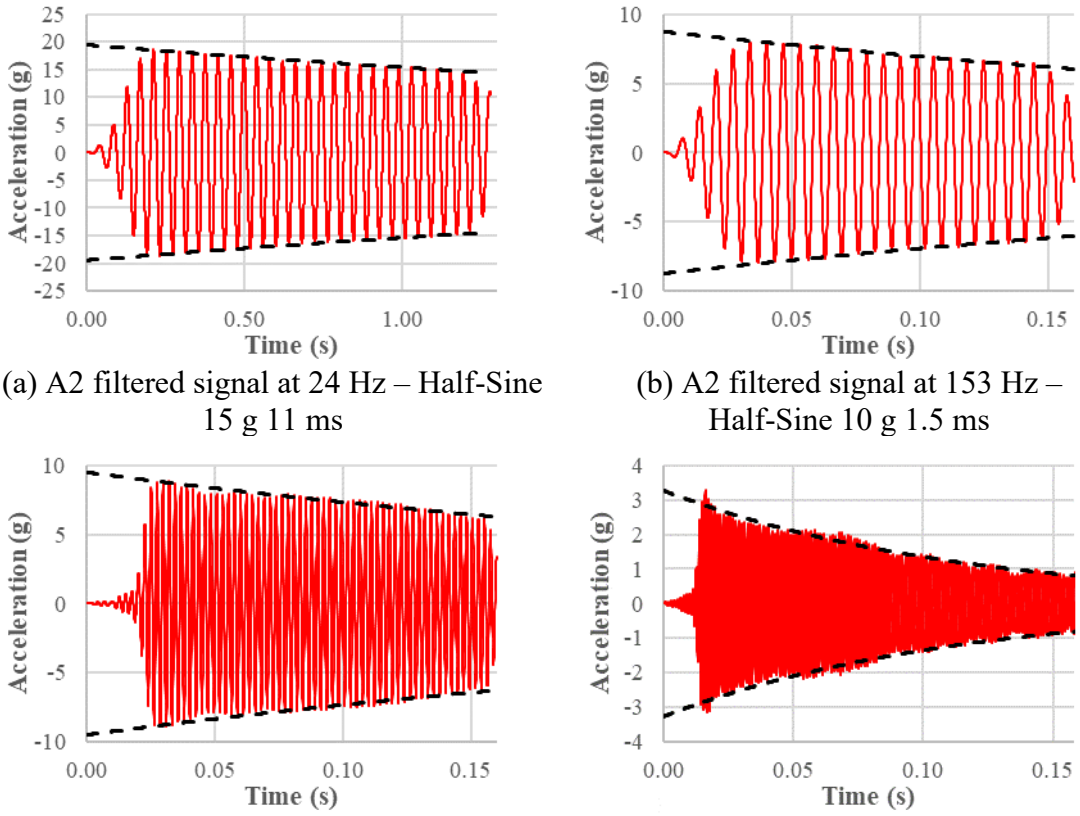

(a) A2 filtered signal at 24 Hz – Half-Sine 15 g 11 ms

(b) A2 filtered signal at 153 Hz – Half-Sine 10 g 1.5 ms

(c) A2 filtered signal at 431 Hz – Rectangular 15 g 1.5 ms

(d) A2 filtered signal at 856 Hz – Terminal 15 g 1.5 ms

Figure 12: Filtered experimental signals and exponential functions that fit the maximum and minimum peaks.

Table 3: Experimental natural frequencies and modal damping ratios for the tested beam.

Experimental natural frequencies (Hz)	Modal damping ratio
24.22	0.18%
153.125	0.26%
431.25	0.10%
856.25	0.16%
1400.0	0.91%

The damping associated with the tested structure can be considered very low (with values less than 1%), so it meets the requirement for this study of being a low damping structure. Other options can be used to calculate the damping coefficients. For example, by performing a sine sweep test, where the damping factor for each natural frequency can be calculated from the maximum peaks of the transmissibility functions by the half-power bandwidth method or other most sophisticated options when the natural frequencies are closer to each other.

2.3 Numerical model description

The results of the analyzed structure subjected to the different shock conditions are also evaluated numerically using finite element simulations in NASTRAN code. The finite element model (FEM) (Figure 13) is composed of 3D elements to represent the

mechanical fixtures and of 2D quadrilateral elements to represent the cantilever beam. The joints between the different parts are modeled by rigid elements (RBE2) and the accelerometers are included as point masses connected to the structure by rigid elements. The numerical accelerations are calculated at the nodes with the point masses that represent the accelerometers.

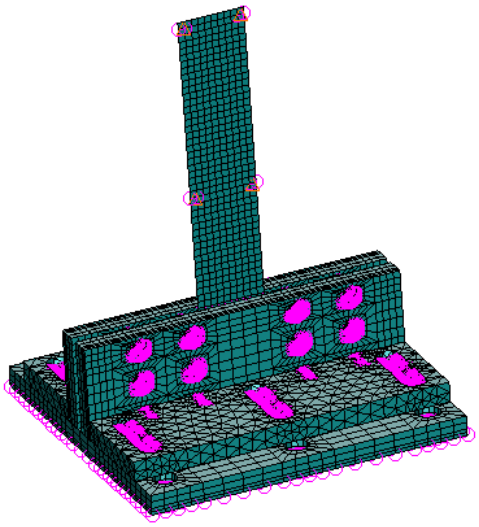

Figure 13: Finite element model of the tested assembly.

This FEM is analyzed to calculate normal modes and acceleration results with the different tested load cases. The modal transient analysis has been used as a solution sequence within the NASTRAN code, defining as input base accelerations the corresponding signals measured by the A1 control accelerometer. The modal damping ratios extracted from the experimental results (see Table 3) are employed in the numerical transient analyses.

3 Results

3.1 Comparison between numerical and experimental results

In this section, the numerical results obtained from the FEM are compared with the experimental results to validate the numerical simulations. The natural frequencies calculated numerically are compared in Table 4 with the experimental modes. It is important to highlight that the experimental modes correspond only to the bending modes that have been excited during the shock tests, while the list of numerical modes also includes torsional modes and bending modes in the perpendicular direction that are not of interest in this study. The differences between the natural frequencies are very low, demonstrating the great similarity between the numerical model and the tested structure.

Table 4: Comparison between the experimental and numerical natural frequencies.

ID	Type	FEM natural frequency (Hz)	Test natural frequency (Hz)	Difference
1	Bending	24.45	24.22	0.95%
2	Bending	151.51	153.125	-1.05%
3	Torsional	205.32		
4	Bending	428.82	431.25	-0.56%
5	Torsional	607.89		
6	Bending (cross direction)	752.83		
7	Bending	861.87	856.25	0.66%
8	Torsional	1105.41		
9	Bending	1402.46	1400.00	0.18%
10	Torsional	1648.91		
11	Bending	2130.69		
12	Torsional	2227.40		
13	Bending	2264.19		

The comparison of the time signals of the response accelerations between the numerical results and the test data is shown in Figure 14, Figure 15 and Figure 16, where it can be appreciated the great similarity of most of the numerical results with respect to the experimental curves. There are some differences with respect to the experimental data for some results (see Figure 15 (e) and (f) and Figure 16 (e) and (f)), which are due to the influence of high-frequency modes whose modal responses have not been represented accurately by the numerical results, due to the lack of accuracy of the FEM approach at high frequencies in some cases.

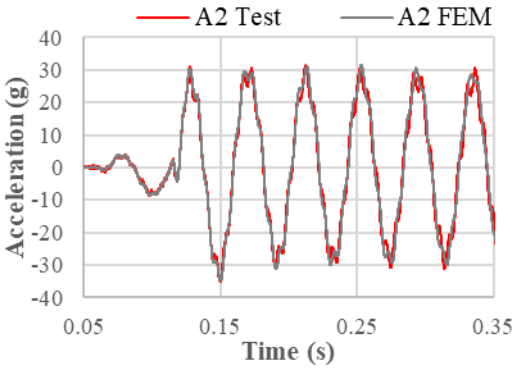

(a) A2 signals – Half-Sine 15 g 11 ms

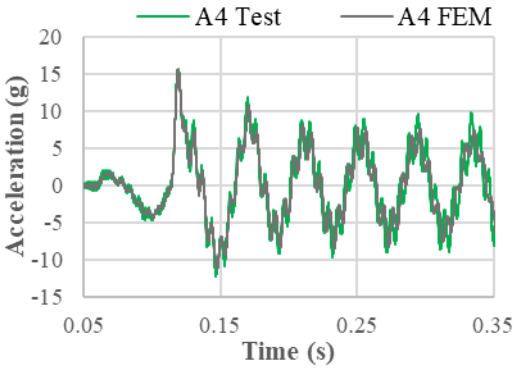

(b) A4 signals – Half-Sine 15 g 11 ms

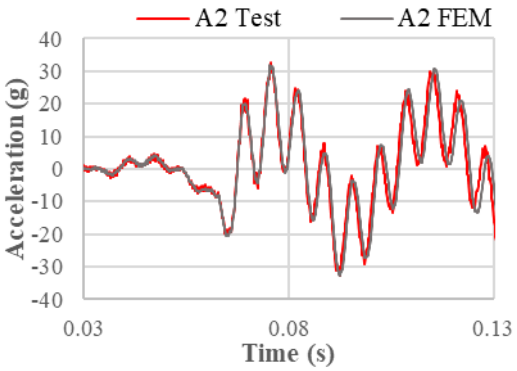

(c) A2 signals – Half-Sine 15 g 6 ms

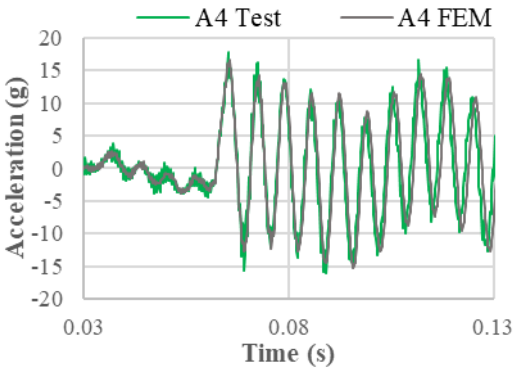

(d) A4 signals – Half-Sine 15 g 6 ms

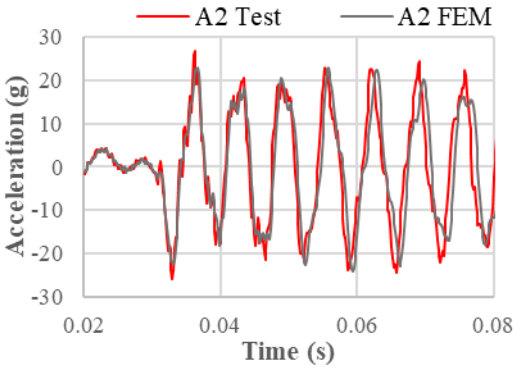

(e) A2 signals – Half-Sine 15 g 3 ms

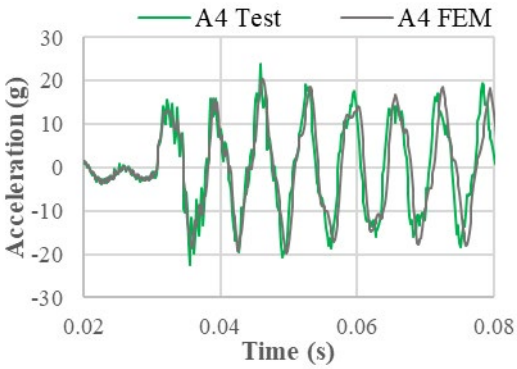

(f) A4 signals – Half-Sine 15 g 3 ms

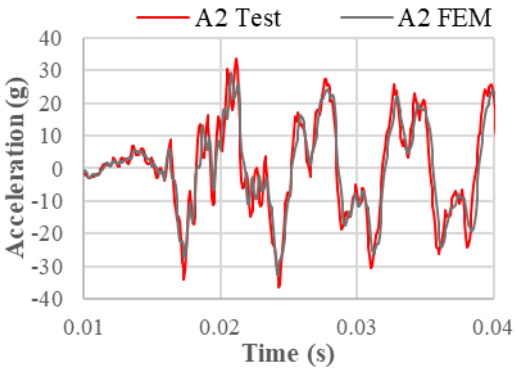

(g) A2 signals – Half-Sine 15 g 1.5 ms

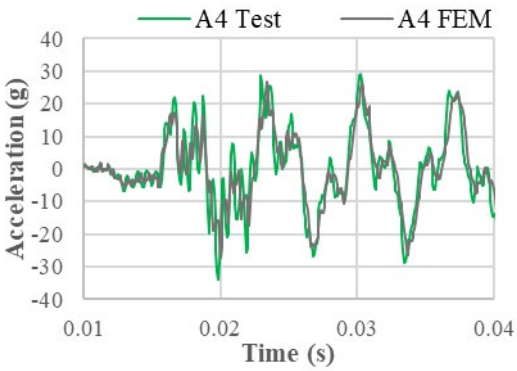

(h) A4 signals – Half-Sine 15 g 1.5 ms

Figure 14: Comparison of response accelerations between FEM and test results – Half-Sine pulse.

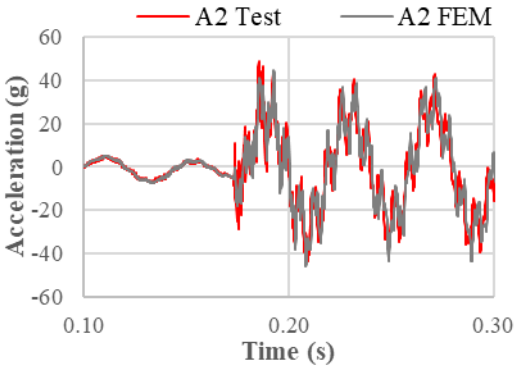

(a) A2 signals – Rectangular 10 g 11 ms

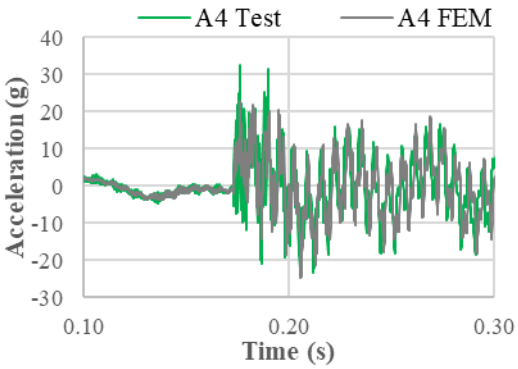

(b) A4 signals – Rectangular 10 g 11 ms

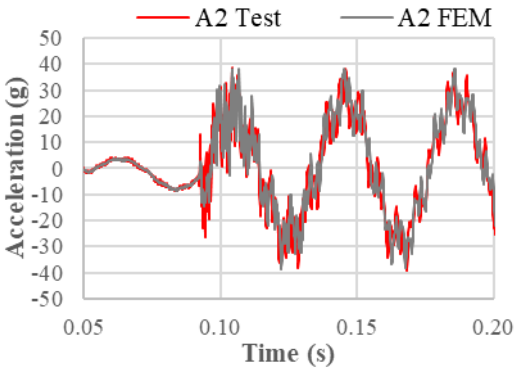

(c) A2 signals – Rectangular 10 g 6 ms

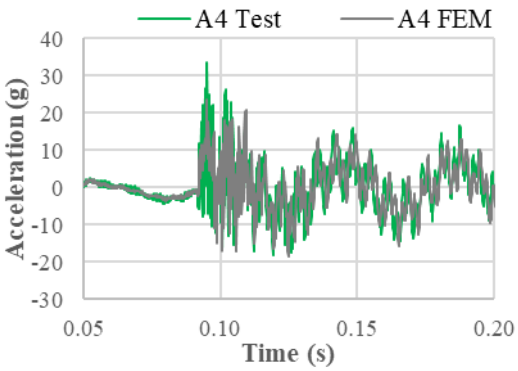

(d) A4 signals – Rectangular 10 g 6 ms

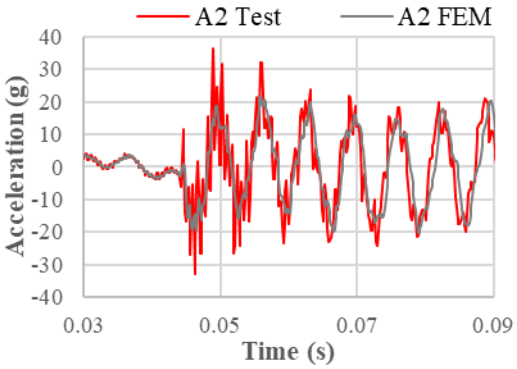

(e) A2 signals – Rectangular 10 g 3 ms

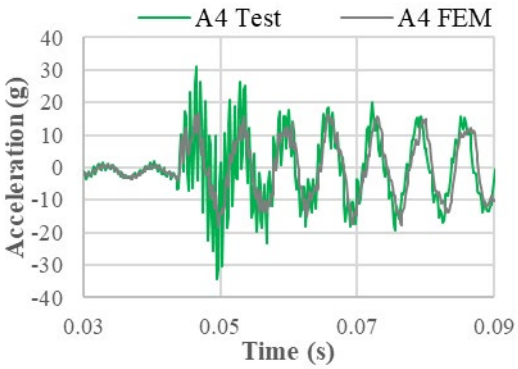

(f) A4 signals – Rectangular 10 g 3 ms

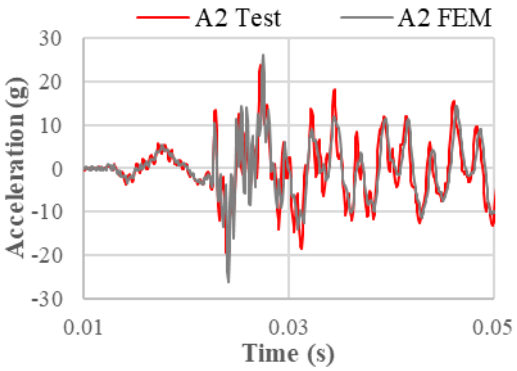

(g) A2 signals – Rectangular 10 g 1.5 ms

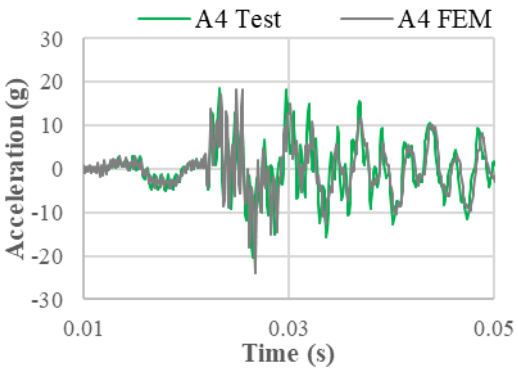

(h) A4 signals – Rectangular 10 g 1.5 ms

Figure 15: Comparison of response accelerations between FEM and test results – Rectangular pulse.

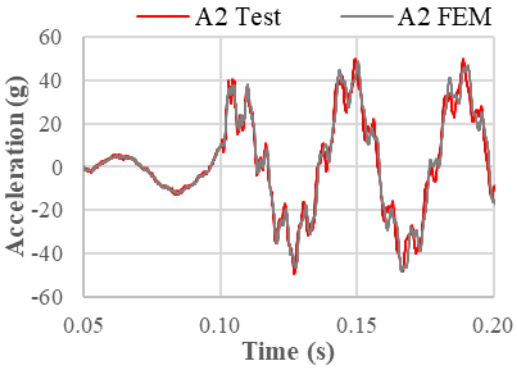

(a) A2 signals – Terminal 15 g 11 ms

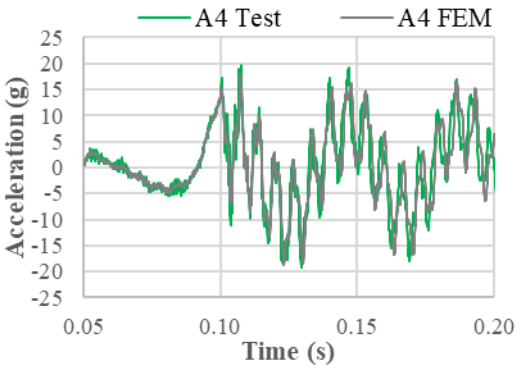

(b) A4 signals – Terminal 15 g 11 ms

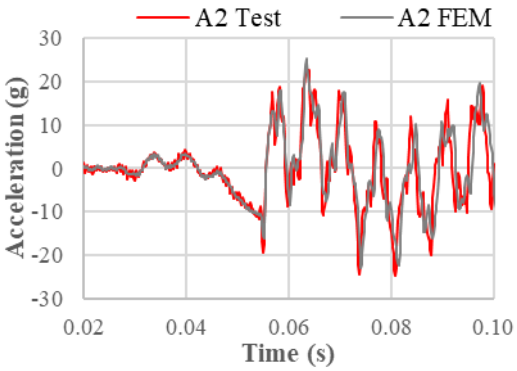

(c) A2 signals – Terminal 15 g 6 ms

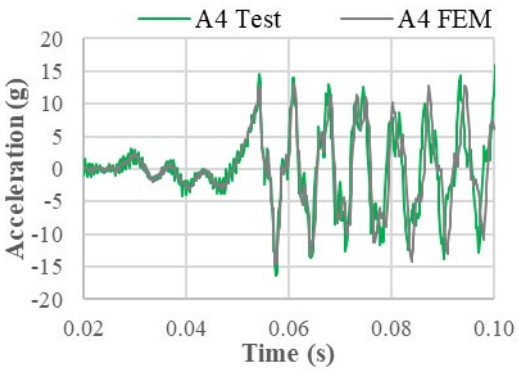

(d) A4 signals – Terminal 15 g 6 ms

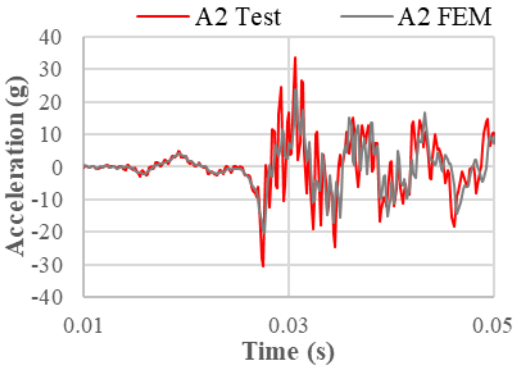

(e) A2 signals – Terminal 15 g 3 ms

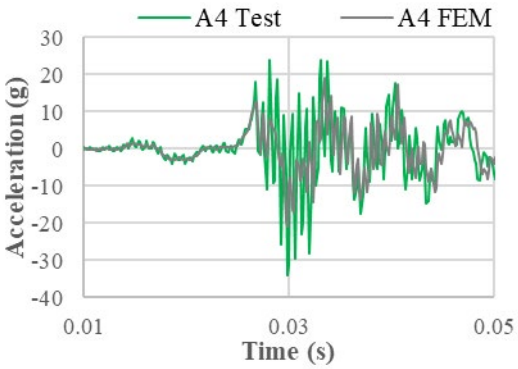

(f) A4 signals – Terminal 15 g 3 ms

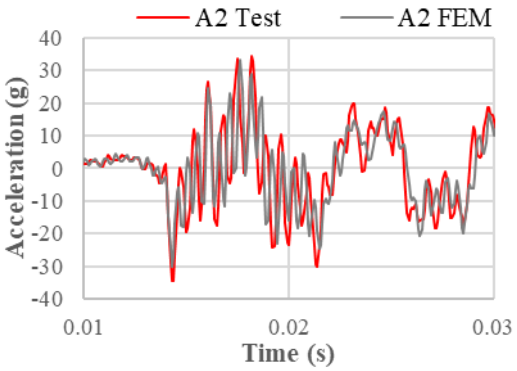

(g) A2 signals – Terminal 15 g 1.5 ms

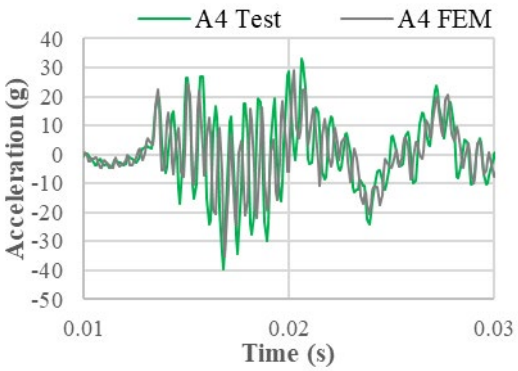

(h) A4 signals – Terminal 15 g 1.5 ms

Figure 16: Comparison of response accelerations between FEM and test results – Terminal sawtooth pulse.

3.2 Modal decomposition of the response accelerations

In this section, the modal contributions to the response accelerations will be assessed to determine the influence of each normal mode on the results. Therefore, each physical response calculated numerically with the FEM will be decomposed into the different modal responses to demonstrate the hypothesis presented in this paper about the classification of normal modes according to the type of modal response generated by a pulsed base acceleration.

The decomposition of the responses into the different modal contributions calculated numerically at the A2 location for the load cases of Half-sine pulse, Rectangular pulse and Terminal peak sawtooth pulse, all with 15 g of amplitude and 1.5 ms of duration for the main pulse, are shown in Figure 17 for the modes belonging to Category 1, Figure 18 for the modes of Category 2 and Figure 19 for the modes of Category 3. It can be clearly seen in Figure 17 how the modal response of the modes of the first category, which for all the examples correspond to the first bending mode, can be considered negligible compared to the other responses. The modes of the second category (see Figure 18) present a damped sinusoidal response after the application of the input pulse, where the maximum and minimum peaks are periodically repeated with low decay. The modal responses of the modes of the third category (see Figure 19) present the maximum peaks just at the instant of the maximum peak of the input acceleration. The peaks for some of these modal responses have the same sign as the input, while for other responses they have the opposite sign. It is also interesting that the response of some of the modes of this third category present a damped sinusoid shape after the input pulse, but with amplitude levels lower than the corresponding maximum peaks produced during the input pulse.

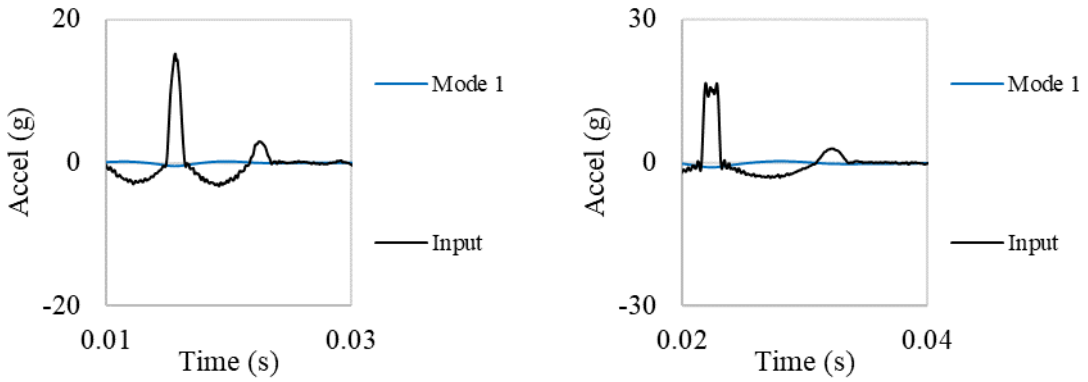

(a) Half-sine 15 g 1.5 ms (b) Rectangular 15 g 1.5 ms

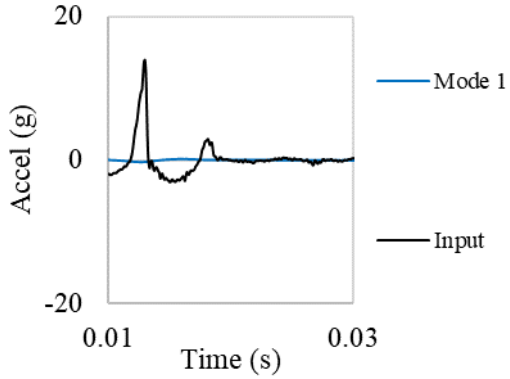

(c) Terminal 15 g 1.5 ms

Figure 17: Modal responses at A2 location for the modes belonging to Category 1.

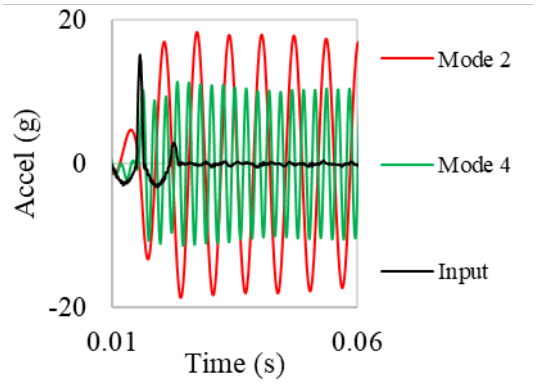

(a) Half-sine 15 g 1.5 ms

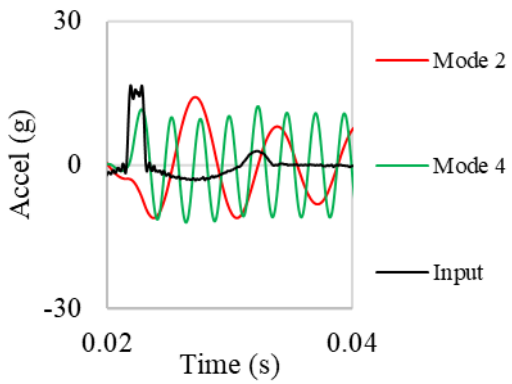

(b) Rectangular 15 g 1.5 ms

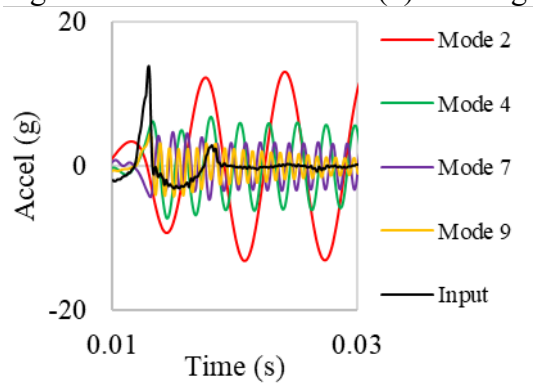

(c) Terminal 15 g 1.5 ms

Figure 18: Modal responses at A2 location for the modes belonging to Category 2.

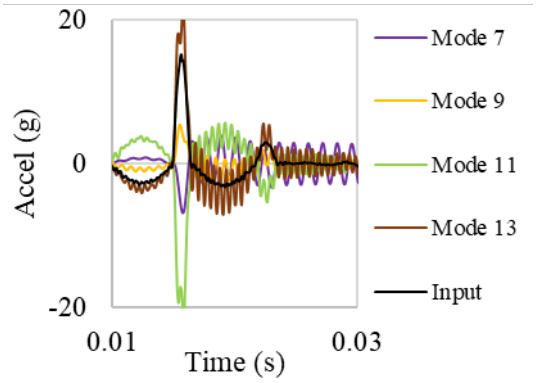

(a) Half-sine 15 g 1.5 ms

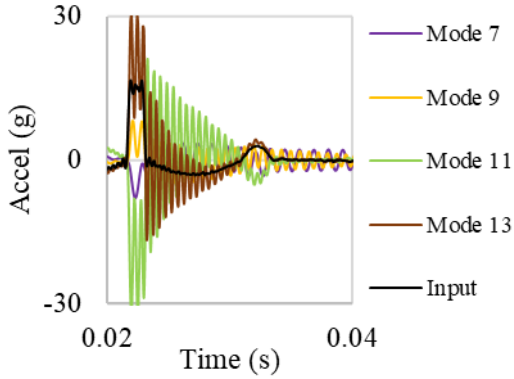

(b) Rectangular 15 g 1.5 ms

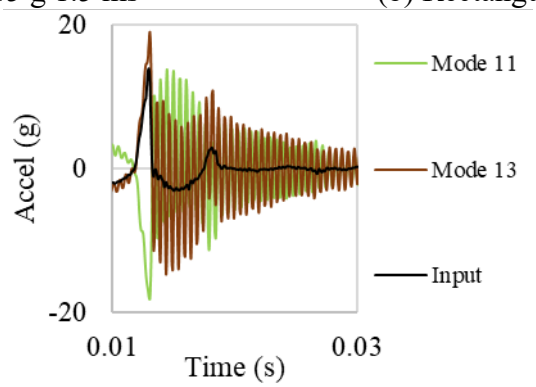

(c) Terminal 15 g 1.5 ms

Figure 19: Modal responses at A2 location for the modes belonging to Category 3.

3.3 Proposed option for the Response Spectrum Analysis

A new method is proposed in this paper to directly predict the maximum peaks of response by an RSA. The RSA approach employs only the information related to the normal modes of the analyzed structure (natural frequencies, modal participation factors and eigenvectors) together with the representation of the input load in terms of SRS, so that it is an alternative technique that achieves these results in a faster way than the transient analysis. In the case that the analyzed model has a non-constant modal damping factor, it is necessary to use more than one curve to represent the input load in the SRS format (see Figure 1), where each curve is related to a different damping or amplification factor. In this paper, all the input signals are converted into SRS curves considering three different values for the amplification factor (10, 50 and 500).

The input SRS together with the response accelerations at the A2 location decomposed into the modal responses are shown in Figure 20, Figure 21 and Figure 22 for the different load cases. Each input SRS is defined by three curves associated with the amplification factors of 10, 50 and 500. In the same graphs, the $SRS\,(f_i)$ values for each mode used in the RSA simulations are indicated with markers. Additionally, in each SRS graph there are three vertical dot-dashed lines located at the limiting frequencies f_1, f_2 and f_3 in increasing order that indicate the different frequency ranges defined in Eqs. (4) and (5) for the IDR-UPM option. These frequencies have been defined according to the shape of the SRS curves, which are described below.

The SRS curves of the pulsed loads are characterized by a low-frequency section up to the first vertical line at f_1 with low values of SRS. The modes of the first category are found in this first section, whose contributions to the responses are considered negligible because their natural frequencies are well below the frequency content of the input acceleration. Between the first (f_1) and the second (f_2) vertical lines, the input SRS curves rise rapidly to their maximum levels, which is a region characterized by humps and valleys in a similar way to the FFT functions of the input signals shown in Figure 9, Figure 10 and Figure 11. A greater difference between the SRS curves associated to the different amplification factors appears at this mid-frequency range, which reveals a greater influence of the damping factor of the model on the response. This aspect is related to the fact that the modes of the second category, whose modal responses are characterized by sinusoidal signals, are found within this frequency range between f_1 and f_2. The maximum peaks of the responses of these modes correspond to any of the first oscillations that usually appear after the input pulse. Therefore, the influence of the damping on the peak values of these responses is more significant than for the responses of the modes of the rest of categories.

As can be seen in Figure 20, Figure 21 and Figure 22, the total responses at the A2 location are mainly dominated by the contributions of the modes of the second category. Therefore, the maximum peak of the total response for each load case is generated after the input pulse, at an instant of time where the peaks of these modal responses coincide with the same sign. Taking into account the low damping values of the analyzed structure, it can be assumed that when this moment occurs, the value of each modal response at this instant is not very different from the absolute maximum peak that may appear at another instant. This assumption is included in the IDR-UPM option in the first summation of Eq. (4), which is the summation of the absolute values of the modal responses for the modes of the second category, between f_1 and f_2.

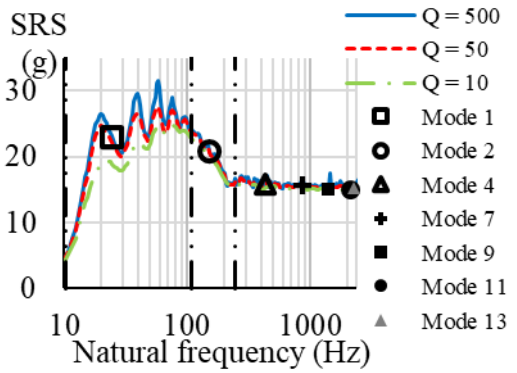

(a) Half-sine 15 g 11 ms – Input SRS

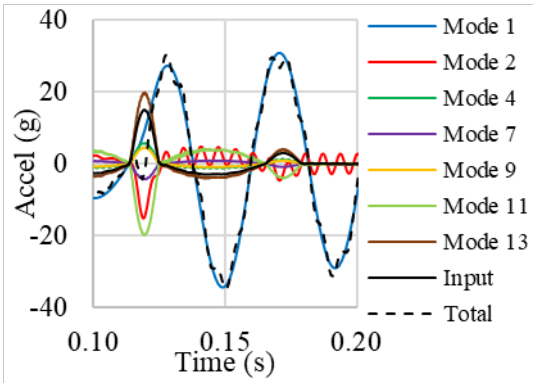

(b) Half-sine 15 g 11 ms – A2 response

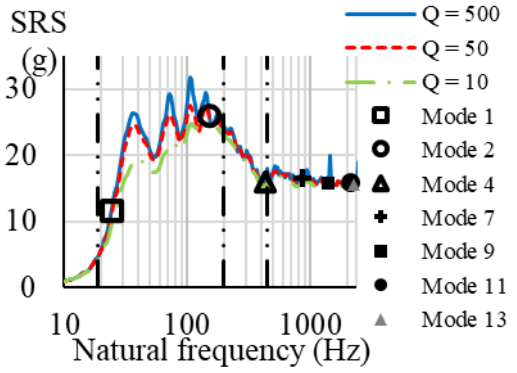

(c) Half-sine 15 g 6 ms – Input SRS

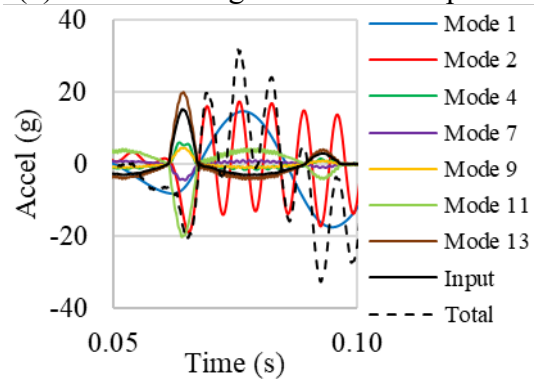

(d) Half-sine 15 g 6 ms – A2 response

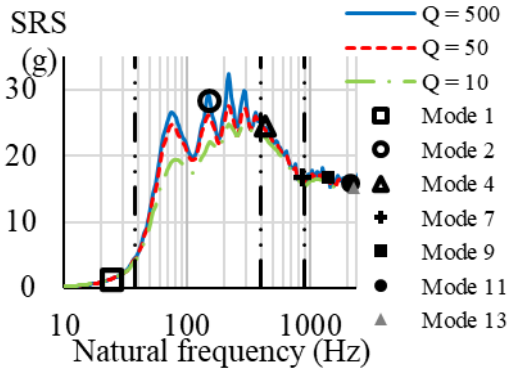

(e) Half-sine 15 g 3 ms – Input SRS

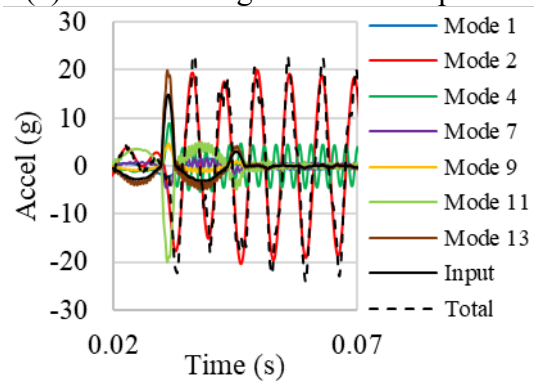

(f) Half-sine 15 g 3 ms – A2 response

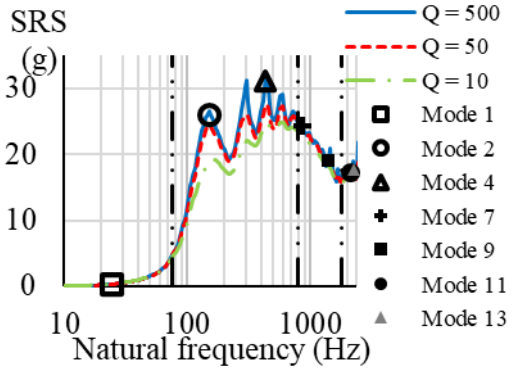

(g) Half-sine 15 g 1.5 ms – Input SRS

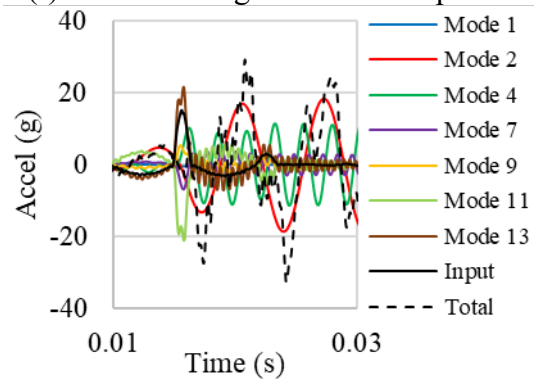

(h) Half-sine 15 g 1.5 ms – A2 response

Figure 20: Input SRS curves and modal responses at A2 location for Half-sine pulse load cases.

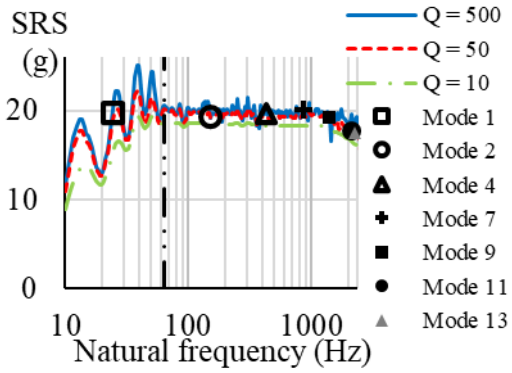

(a) Rectangular 10 g 11 ms – Input SRS

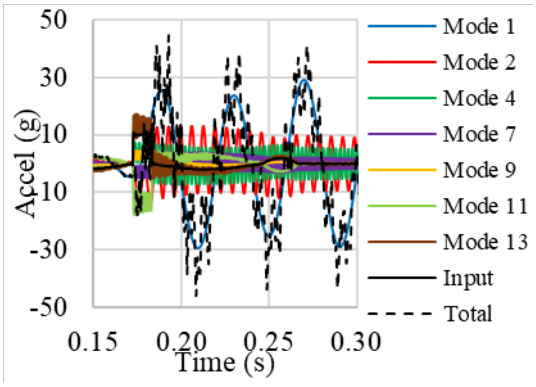

(b) Rectangular 10 g 11 ms – A2 response

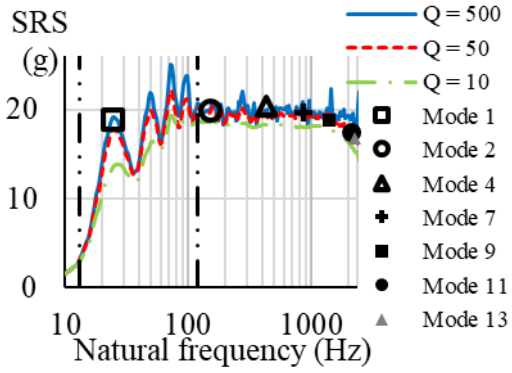

(c) Rectangular 10 g 6 ms – Input SRS

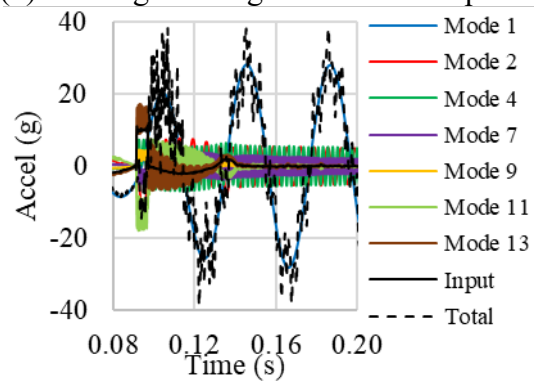

(d) Rectangular 10 g 6 ms – A2 response

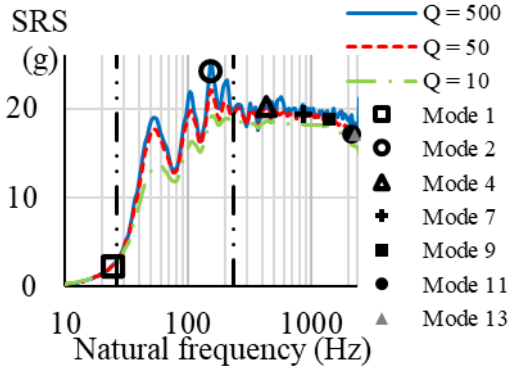

(e) Rectangular 10 g 3 ms – Input SRS

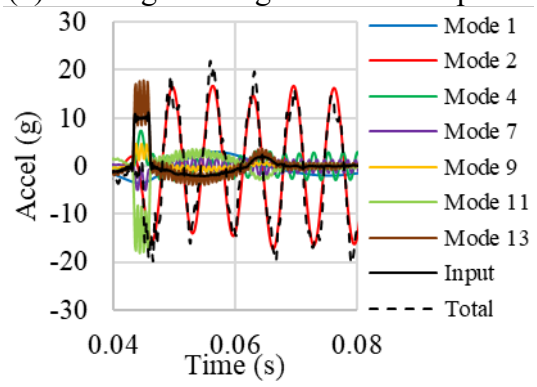

(f) Rectangular 10 g 3 ms – A2 response

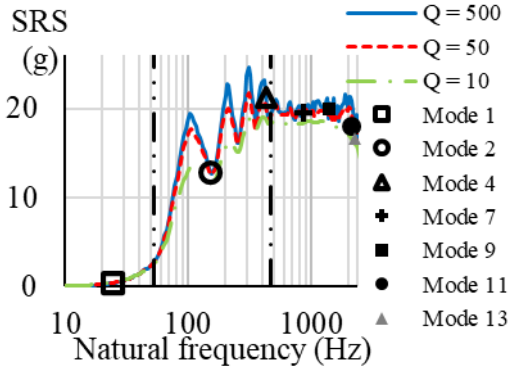

(g) Rectangular 10 g 1.5 ms – Input SRS

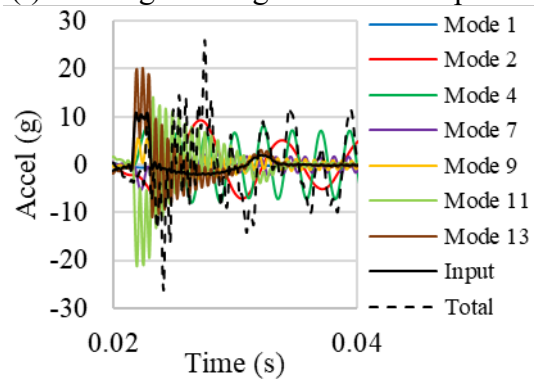

(h) Rectangular 10 g 1.5 ms – A2 response

Figure 21: Input SRS curves and modal responses at A2 location for Rectangular pulse load cases.

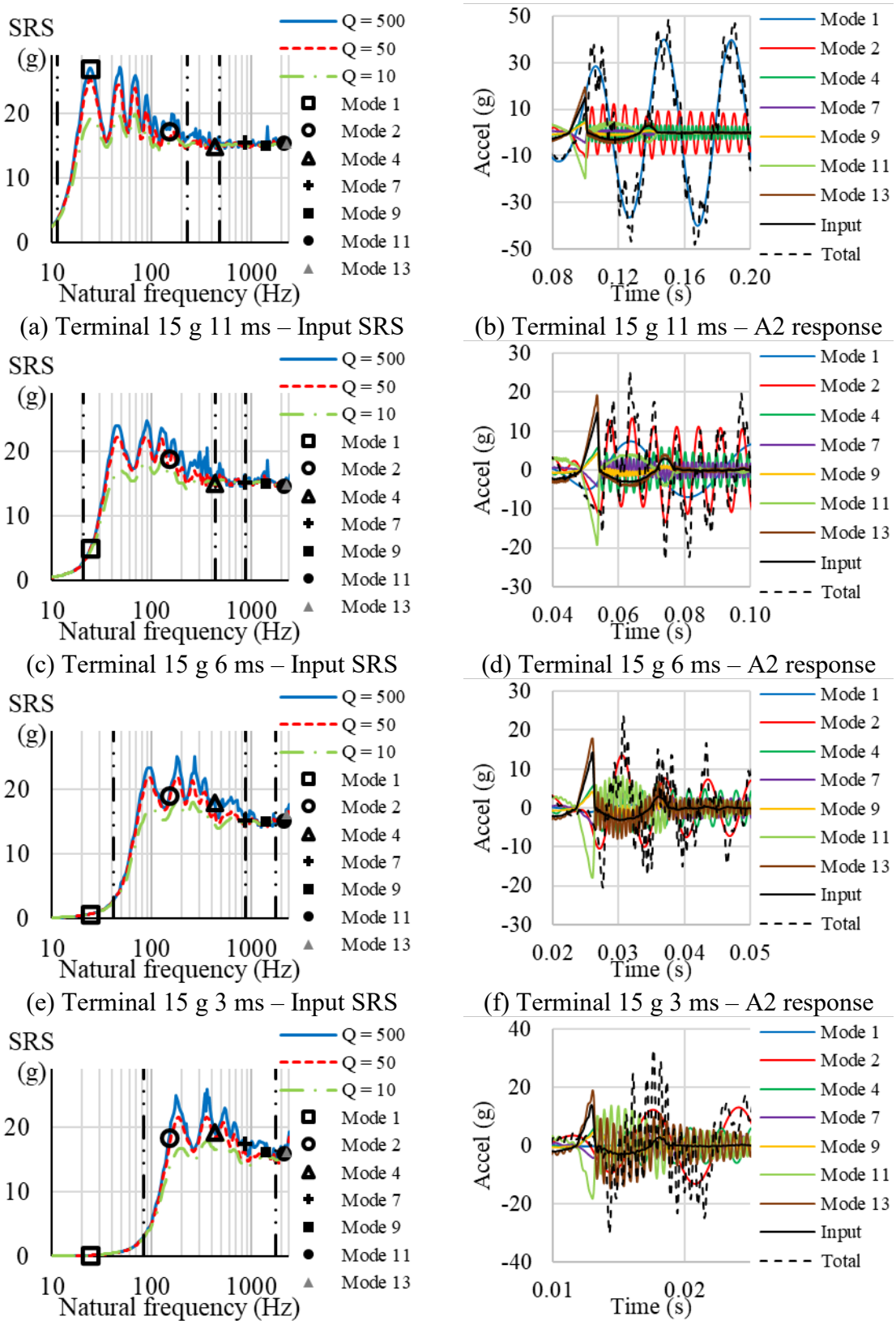

(a) Terminal 15 g 11 ms – Input SRS

(b) Terminal 15 g 11 ms – A2 response

(c) Terminal 15 g 6 ms – Input SRS

(d) Terminal 15 g 6 ms – A2 response

(e) Terminal 15 g 3 ms – Input SRS

(f) Terminal 15 g 3 ms – A2 response

(g) Terminal 15 g 1.5 ms – Input SRS

(h) Terminal 15 g 1.5 ms – A2 response

Figure 22: Input SRS curves and modal responses at A2 location for Terminal sawtooth pulse load cases.

The modes of the third category, whose modal responses are characterized by shapes like the input pulse, with the maximum peak at the same instant, are in the high-frequency range after f_2. There is a transition zone for the input SRS of the Half-sine

pulse and Terminal sawtooth pulse defined between the second (f_2) and the third (f_3) vertical lines. For the Half-sine pulse (see Figure 20), this transition region is characterized by the decrease of the SRS curves from the middle zone to the last region with horizontal SRS curves. There also exist intermediate regions for the Terminal sawtooth pulses (see Figure 22), but they are not as clear as for the Half-sine pulses. The modal responses of the modes found in these intermediate regions have the same shape as the input pulse during its application, followed by a subsequent damped sinusoidal oscillation for the later time. Taking into account that these modes belong to the third category, the maximum peaks of their responses are generated at the same instant of the maximum value of the input pulse, but their subsequent sinusoidal oscillations are also significant for the calculation of the total peak value for the time after the input pulse in Eq. (4). In this equation, the contribution of the modes of the transition region (between f_2 and f_3) is considered in the second summation, but with the application of a correction factor K_1 related to the ratio between the amplitude value of the sinusoidal oscillation of the response after the input pulse and the maximum peak of the response generated during the input pulse. For the rectangular pulses (see Figure 21), the transition region extends to the last frequency of interest considered in the simulations performed in this study.

Finally, the SRS curves of the Half-sine (see Figure 20) and Terminal sawtooth (see Figure 22) pulses are characterized by a horizontal asymptotic behavior in the high-frequency region above f_3 towards certain values. Each of these values precisely coincides with the maximum value of the input pulse, which corresponds to 15 g for both mentioned examples, due to the fact that a SDOF system whose natural frequency is far above the frequency content of the input load generates a response with the same shape and intensity as the input acceleration. Consequently, the modal responses of the modes of the third category that belong to this high-frequency region above f_3 have the same characteristics. For the time after the application of the input pulse, these modal responses can be considered negligible, and therefore, they are not considered in Eq. (4) for the proposed IDR-UPM option. However, during the input pulse, each response reaches its peak value, which can be negative or positive depending on the sign of the product between the modal participation factor and the component of the eigenvector (see Eq. (2)). These peak values are taken into account for the IDR-UPM option in the second summation in Eq. (5), as the main contribution to the peak value of the physical response generated during the input pulse. The modes of the second category are also taken into account in this equation in the first summation, where each modal contribution is multiplied by a scale factor K_i that depends on the ratio between the value of the modal response at the instant of the input pulse and the maximum peak value generated later. The accurate determination of the values of these scale factors to be applicable to other type of structures has not been studied in depth yet in this work, but they can be initially estimated by evaluating separately each modal contribution of the analyzed structure. In Eq. (5), the modal contributions are algebraically summed taking into account the different signs of the peak responses generated during the input pulse.

The relationship between the limiting frequencies f_1, f_2 and f_3 and the duration in seconds of the main pulse (T) can be defined with the next equation, where the empirical values found in this study for the constants C_i are indicated in Table 5.

$$f_i = \frac{C_i}{T} \tag{6}$$

Table 5: Empirical values for the constants C_i.

Pulse shape	C_1	C_2	C_3
Half-sine	112.5	1192.5	2700
Rectangular	79	711	-
Terminal sawtooth	125	2500	5250

The comparison between the maximum peak values for the response accelerations at the A2 location calculated with the different numerical options is shown in Table 6. For all the IDR-UPM results, the maximum peak values have been calculated considering Eq. (4), with $K_1 = 0.2$, which has been determined empirically in this structure to have the smallest average error considering all the different load conditions. The results of the transient analysis are considered as a reference to calculate the differences in decibels (see Table 7) of the results from the different RSA options.

Table 6: Maximum peak values for the acceleration response at A2 location calculated by different methods.

Load case	Maximum peak accelerations at A2 location (g)				
	Transient	ABS	NRL	SRSS	IDR-UPM
HS 15g 11ms	34.6	104.3	67.5	47.8	37.4
HS 15g 6ms	32.7	93.5	55.2	40.1	37.6
HS 15g 3ms	24.1	82.7	52.0	37.4	23.3
HS 15g 1.5ms	32.8	89.7	56.3	40.4	33.1
R 10g 11ms	46.0	108.9	66.9	47.6	45.4
R 10g 6ms	38.6	106.8	65.0	46.4	44.0
R 10g 3ms	21.9	85.1	53.5	38.2	30.4
R 10g 1.5ms	26.1	75.1	50.1	35.5	28.8
TS 15g 11ms	48.9	107.8	72.5	51.6	53.7
TS 15g 6ms	25.4	74.6	45.9	32.8	27.7
TS 15g 3ms	23.7	71.5	47.1	33.5	25.8
TS 15g 1.5ms	33.1	72.9	48.1	34.2	38.8

Table 7: Differences (dB) between RSA results and transient analysis results.

Load Case	Differences (dB)			
	ABS	NRL	SRSS	IDR-UPM
HS 15g 11ms	9.57	5.80	2.79	0.67
HS 15g 6ms	9.13	4.55	1.78	1.23
HS 15g 3ms	10.70	6.67	3.81	-0.28
HS 15g 1.5ms	8.75	4.70	1.82	0.09
R 10g 11ms	7.48	3.25	0.30	-0.12
R 10g 6ms	8.84	4.53	1.59	1.13
R 10g 3ms	11.79	7.75	4.84	2.85
R 10g 1.5ms	9.17	5.66	2.66	0.86
TS 15g 11ms	6.86	3.42	0.46	0.81
TS 15g 6ms	9.36	5.14	2.22	0.75
TS 15g 3ms	9.61	5.98	3.01	0.75
TS 15g 1.5ms	6.86	3.24	0.29	1.37
Average	9.01	5.06	2.13	0.84

As can be seen in Table 7, the results of the proposed IDR-UPM option are more accurate than those of the rest of methods, with an average difference below 1 dB. The ABS option presents the highest results, well above the results of transient analysis with errors that exceed 6 dB. The SRSS option is the best of the existing methods for the analyzed structure, but it is not as accurate as the proposed IDR-UPM option. Therefore, it is demonstrated that the IDR-UPM option provides the best predictions of peak acceleration responses in RSA simulations for undamped and low damped structures subjected to impact base accelerations characterized by a main pulse, achieving a remarkable improvement on the level of accuracy of the results calculated by the RSA approach.

4 Conclusions

In this paper, a new method named IDR-UPM has been developed and verified for the accurate calculation of the peak values of the acceleration response in Response Spectrum Analysis simulations of a low damping structure subjected to an impact base acceleration defined by a main pulse. This method has been proposed according to a set of hypotheses that have been demonstrated by an exhaustive study about the contribution of each mode to the response of the structure.

The analyzed structure in this work is a cantilever beam that has first been tested by an electrodynamic shaker, which has generated different input shocks characterized by a main pulse. Each input pulse is defined by its shape (half-sine, rectangular or terminal peak sawtooth), its amplitude (15, 10 or 5 g) and its duration (11, 6, 3 or 1.5 ms). This wide variety of input conditions has allowed a better assessment about their influence on the structural responses. The natural frequencies and the modal damping factors of the tested structure have been determined from the experimental results by using different signal processing techniques, such as the FFT and the band-pass filtering, revealing the low damping values of the analyzed structure. Then, a numerical model of the tested assembly has been created and analyzed to calculate the numerical results under the different shock conditions. The FEM has been validated in this work by showing the great similarity between the numerical and the experimental results in terms of natural frequencies and time functions of the response accelerations. This FEM has been used to decompose each physical response into the different modal contributions, which has been useful in the development of the proposed method. The evaluation of these modal contributions has helped in estimating the value of the correction factor used with the proposed method, but the calculation of these correction factors needs an in-depth study to have generic values that can be applicable to a great variety of structures. Finally, the accuracy of the results calculated by the proposed method has been demonstrated by comparing with the results of the transient analyses, concluding that the proposed IDR-UPM option provides the most accurate results compared to the existing options for the RSA simulations of low damped structures. This method has been specifically developed to evaluate the maximum structural responses generated by shock loads characterized by a main pulse, which is one of the most used ways in the aerospace industry to qualify electronic equipment. Although this method has the limitation of not being applicable to more complex shock environments, such as those generated by impact or detonation tests, it is very attractive to predict mechanical responses against pulse-like shocks quickly and accurately to know if the analyzed system can withstand the severe shock environment before subjecting it to these shock tests.

Acknowledgments

This work has been performed thanks to the help and support of the professors and staff of the Department of Mechanical and Aerospace Engineering at La Sapienza University, in Rome.

Funding: This work has been supported by the "Ayudas a PDI e investigadores doctores para realizar Estancias de Investigación Internacional" of the economic program "Programa Propio UPM 2019" of the Universidad Politécnica de Madrid (UPM).

Declaration of interest

None

References

[1] J.J. Wijker, Spacecraft structures, Springer Berlin Heidelberg, Berlin, Heidelberg, 2008. https://doi.org/10.1007/978-3-540-75553-1.

[2] C. Lalanne, Mechanical Shock Volume II, 2002.

[3] ECSS, ECSS-E-HB-32-25A, Space engineering, Mechanical shock design and verification handbook, ESA-ESTEC Requirements and Standards Division, Noordwijk, The Netherlands, 2015.

[4] A. García-Pérez, A. Ravanbakhsh, F. Sorribes-Palmer, G. Alonso, Structural shock verification by numerical analysis of the EPD payload units on board Solar Orbiter spacecraft, Acta Astronaut. 168 (2020) 282–292. https://doi.org/10.1016/j.actaastro.2019.12.026.

[5] A. García-Pérez, F. Sorribes-Palmer, G. Alonso, A. Ravanbakhsh, Overview and application of FEM methods for shock analysis in space instruments, Aerosp. Sci. Technol. 80 (2018) 572–586. https://doi.org/10.1016/j.ast.2018.07.035.

[6] A. García-Pérez, F. Sorribes-Palmer, G. Alonso, A. Ravanbakhsh, FEM simulation of space instruments subjected to shock tests by mechanical impact, Int. J. Impact Eng. 126 (2019) 11–26. https://doi.org/10.1016/j.ijimpeng.2018.12.008.

[7] H. Zhao, J. Ding, W. Zhu, Y. Sun, Y. Liu, Shock response prediction of the typical structure in spacecraft based on the hybrid modeling techniques, Aerosp. Sci. Technol. 89 (2019) 460–467. https://doi.org/10.1016/j.ast.2019.04.018.

[8] X. Wang, Z. Qin, J. Ding, F. Chu, Finite element modeling and pyroshock response analysis of separation nuts, Aerosp. Sci. Technol. 68 (2017) 380–390. https://doi.org/10.1016/j.ast.2017.05.028.

[9] F. Sánchez Iglesias, A. Fernández López, Rayleigh damping parameters estimation using hammer impact tests, Mech. Syst. Signal Process. 135 (2020). https://doi.org/10.1016/j.ymssp.2019.106391.

[10] C. Riso, S. Fransen, F. Mastroddi, G. Coppotelli, F. Trequattrini, A. De Vivo, Experimental validation of solid rocket motor damping models, CEAS Sp. J. 10 (2018) 213–230. https://doi.org/10.1007/s12567-017-0191-3.

[11] F. Mastroddi, F. Martarelli, M. Eugeni, C. Riso, Time- and frequency-domain linear viscoelastic modeling of highly damped aerospace structures, Mech. Syst. Signal Process. 122 (2019) 42–55. https://doi.org/10.1016/j.ymssp.2018.12.023.

[12] M.A. Biot, Transient oscillations in elastic systems, California Institute of Technology, 1932.

[13] ECSS, ECSS-E-ST-32-03C, Space engineering, Structural finite element models, ESA-ESTEC Requirements and Standards Division, Noordwijk, The Netherlands, 2008.
[14] X. Zhou, R. Yu, D. Dong, Complex mode superposition algorithm for seismic responses of non-classically damped linear MDOF system, J. Earthq. Eng. 8 (2004) 597–641. https://doi.org/10.1142/S1363246904001602.
[15] R. Yu, X. Zhou, Simplifications of CQC method and CCQC method, Earthq. Eng. Eng. Vib. 6 (2007) 65–76. https://doi.org/10.1007/s11803-007-0640-7.
[16] R. Yu, X. Zhou, A. Abduwahit, Complex complete quadratic combination method for damped system with repeated eigenvalues, J. Earthq. Eng. Eng. Vib. 15 (2016) 537–550. https://doi.org/10.1007/s11803-016-0342-0.
[17] H. Chen, P. Tan, F. Zhou, An improved response spectrum method for non-classically damped systems, Bull. Earthq. Eng. 15 (2017) 4375–4397. https://doi.org/10.1007/s10518-017-0144-4.
[18] Y. Yan, Q.M. Li, Low-pass-filter-based shock response spectrum and the evaluation method of transmissibility between equipment and sensitive components interfaces, Mech. Syst. Signal Process. 117 (2019) 97–115. https://doi.org/10.1016/j.ymssp.2018.07.023.